Supernova Type Ia Luminosities, Their Dependence on Second Parameters, and the Value of H_0

B. R. Parodi[1], A. Saha[2], A. Sandage[3], and G. A. Tammann[1]

ABSTRACT

A sample of 35 SNe Ia with good to excellent photometry in B and V, minimum internal absorption, and $1200 < v \lesssim 30\,000\,\mathrm{km\,s^{-1}}$ is compiled from the literature. As far as their spectra are known they are all Branch-normal. For 29 of the SNe Ia also peak magnitudes in I are known. The SNe Ia have uniform colors at maximum, i.e. $<B\text{-}V>=-0^m.012$ (σ=0.051) and $<V\text{-}I>=-0^m.276$ (σ=0.078). In the Hubble diagram they define a Hubble line with a scatter of $\sigma_M=0^m.21$-$0^m.16$, decreasing with wavelength. The scatter is further reduced if the SNe Ia are corrected for differences in decline rate Δm_{15} or color $(B-V)$. A combined correction reduces the scatter to $\sigma \lesssim 0^m.13$. After the correction no significant dependence remains on Hubble type or galactocentric distance. The Hubble line suggests some curvature which can be differently interpreted. A consistent solution is obtained for a cosmological model with Ω_M=0.3, Ω_Λ=0.7, which is indicated also by much more distant SNe Ia. Absolute magnitudes are available for eight equally blue (Branch-normal) SNe Ia in spirals, whose Cepheid distances are known. If their well defined mean values of M_B, M_V, and M_I are used to fit the Hubble line to the above sample of SNe Ia one obtains H_0=58.3 $\mathrm{km\,s^{-1}\,Mpc^{-1}}$, or, after adjusting all SNe Ia to the average values of Δm_{15} and $(B-V)$, H_0=60.9 $\mathrm{km\,s^{-1}\,Mpc^{-1}}$. Various systematic errors are discussed whose elimination tends to decrease H_0. The finally adopted value at the 90-percent level, including random and systematic errors, is $H_0=58.5\pm6.3$ $\mathrm{km\,s^{-1}\,Mpc^{-1}}$. Several higher values of H_0 from SNe Ia, as suggested in the literature, are found to depend on large corrections for variations of the light curve parameter and/or on an unwarranted reduction of the Cepheid distances of the calibrating SNe Ia.

Subject headings: supernovae: general—cosmology: distance scale

[1]Astronomisches Institut der Universität Basel, Venusstr. 7, CH-4102 Binningen, Switzerland; parodi@astro.unibas.ch.

[2]National Optical Astronomy Observatories, 950 North Cherry Avenue, Tucson, AZ 85726-6732, USA; saha@noao.edu.

[3]The Observatories of the Carnegie Institution of Washington, 813 Santa Barbara Street, Pasadena, CA 91101-1292, USA.

1. Introduction

Supernovae of type Ia (SNe Ia) are the prime distance indicators for the determination of the Hubble constant H_0 since they can be followed out to large distances, and since it is possible to determine Cepheid distances with HST for the nearest of their host galaxies and hence to calibrate their luminosity at maximum (Sandage et al. 1992). This immediately yields the distances of the more distant SNe Ia because they are – if restricted to blue objects – the best standard candles known with a luminosity scatter of less than $\sigma_M = 0\overset{m}{.}25$. As standard candles they are now so heavily relied upon that they are even used for the much more sensitive test for the cosmological constant Λ (Riess et al. 1998b; Perlmutter et al. 1999). A wealth of excellent photometric data for SNe Ia has been accumulated since 1985 by the Calán/Tololo team (Hamuy et al. 1996b) and others. They reach out to $\sim 30\,000$ km s^{-1}, i.e. far enough to avoid the effects of peculiar and streaming motions. In parallel, the HST Supernova Project has by now provided Cepheid-calibrated luminosities for six nearby SNe Ia (Saha et al. 1999), not counting SN 1895 B for which only the B magnitude is known. These are augmented by two additional calibrators from Tanvir et al. (1995) and Turner et al. (1998). With a total of eight calibrators and three dozen more distant SNe Ia, the statistics rests on solid ground.

The one remaining question is whether the calibrators and the distant SNe Ia are genuine twins, or whether the different selection criteria cause systematic differences between the samples. For instance, the Cepheid distances of the calibrators imply that they lie in galaxies containing young-population stars, whereas the distant SNe Ia have also been observed in S0 and E galaxies. Various second parameters have been proposed to correlate with SN luminosity; they can serve as a control of luminosity differences between the nearby calibrators and the distant SNe Ia. From the point of view of the physicist the most interesting second parameters are several spectral features which are known to correlate with luminosity (Nugent et al. 1995; Fisher et al. 1995, 1999; Riess et al. 1998a; Mazzali et al. 1998). But the available data are too sparse to be useful in the present context. One is therefore reduced to empirical second parameters such as light curve shape, SN color, Hubble type and position in the parent galaxy. Second parameters have been discussed by, e.g., Phillips (1993); Tammann & Sandage (1995); Vaughan et al. (1995); Hamuy et al. (1996a,c); Tripp (1998); Tripp & Branch (1999); Saha et al. (1999); Riess et al. (1999); Jha et al. (1999); Phillips et al. (1999); Suntzeff et al. (1999); Gibson et al. (2000a).

The difficulty to find a correlation between SN Ia luminosities and the second parameters in face of an intrinsic scatter of $\sigma_M \lesssim 0\overset{m}{.}25$ is that very accurate *relative* distances are required. Cepheid distances and, e.g., Tully-Fisher distances are not sufficiently accurate for the purpose. SNe Ia in the Virgo cluster cannot be assumed to lie at the same distance because of the important depth effect of the cluster. Regress must therefore be taken to the *relative* distances that are indicated by recession velocities. All velocities $v > 1200$ km s^{-1} are taken as indicative of the relative distances. This is permissible because the errors assigned to the relative distances and to the resulting relative absolute magnitudes make allowance for reasonable values of the peculiar velocities (Section 2.1).

The purpose of the present paper is to discuss the correlation of second parameters with the peak luminosity of SNe Ia — using an enlarged and well-defined sample of distant SNe Ia — and to determine the value of the Hubble constant. The SNe Ia magnitudes, after correction for decline rate Δm_{15} and color (B-V), have a scatter of only $\sigma_M \lesssim 0\overset{m}{.}13$. In fact the magnitude-corrected SNe Ia define the Hubble diagram so well that a flat Universe model with Ω_M=0.3, Ω_Λ=0.7 gives a marginally better fit than an Ω_M=1 model. The corrected magnitudes, if combined with the corrected absolute magnitudes of eight Cepheid-calibrated SNe Ia, determine H_0 with a very small *statistical* error.

The organization of the present paper is as follows. In Section 2 the available data for blue SNe Ia are compiled, and their luminosity calibration by means of eight SNe Ia with known Cepheid distances is discussed. The SNe Ia colors and extinctions are discussed in Section 3. The Hubble diagram is shown in Section 4. In Section 5 the SN Ia luminosities are discussed in function of decline rate Δm_{15}, SN color (B-V), Hubble type T, and position in the parent galaxy. The effective Hubble diagram with decline-rate and color corrected magnitudes is shown in Section 6, and the resulting values of H_0 are derived. Alternative solutions are explored in Section 7, and the conclusions are given in Section 8.

2. The Photometric Data

2.1. Blue SNe Ia within v $\lesssim$ 30 000 km s^{-1}

The available data for all SNe Ia (n=67) with (B_{max}-V_{max})≤ 0.20[4] (after correction for Galactic reddening following Schlegel et al. (1998)), and with $v \lesssim 30\,000\,\mathrm{km\,s^{-1}}$ (the two largest accepted velocities are $v = 30\,269\,\mathrm{km\,s^{-1}}$ of SN 1992 aq and $v = 37\,325\,\mathrm{km\,s^{-1}}$ of SN 1996 ab) are compiled in Table 1.

The individual columns bear the following informations:
(1): The supernova designation. If followed by an acceptance sign $\surd$ the SN is included in the fiducial sample (see below). **(2)**: The Hubble type of the parent galaxy as coded by de Vaucouleurs (1974), but slightly simplified for the early and latest types: E: T=-3; E/S0: T=-2; S0: T=-1; S0/a: T=0; Sa: T=1; Sab: T=2; Sb: T=3; Sbc: T=4; Sc,Sd,Sm & Im: T=5. The Am galaxy NGC 5253 (SN 1972 E) has tentatively been ascribed the type T=5. **(3)**: The decimal logarithm of the galaxy redshift velocity cz. Most redshifts are from the Lyon/Meudon Extragalactic Database (LEDA; http://www-obs.univ-lyon1.fr); additional redshifts were taken from Hamuy et al. (1996b) and Riess et al. (1999). They were corrected for the motion of the Sun relative to the centroid of the local group (Yahil et al. 1977) and for a self-consistent Virgocentric infall model with a local infall vector of 220 km s^{-1} (Kraan-Korteweg 1986); beyond $v_{220} = 3000\,\mathrm{km\,s^{-1}}$ an additional correction

[4]In the following we write for (B_{max}-V_{max}) and (V_{max}-I_{max}) more conveniently (B-V) and (V-I).

for the motion of 630 km s^{-1} relative to the CMB dipole anisotopy (Smoot et al. 1992) was applied. Varying the size of the local co-moving volume between 2000 and 10 000 km s^{-1} has no significant effect on the present conclusions. For the members of three clusters the following mean velocities were assumed: for Cen A group members v_{220} = 291 km s^{-1} (Kraan-Korteweg 1986), for Virgo cluster members, as assigned by Binggeli et al. (1993), v_{220} = 1179 km s^{-1} (Jerjen & Tammann 1993), for Fornax cluster members, as assigned by Ferguson & Sandage (1988), v_{220} = 1440 km s^{-1} (Tammann & Federspiel 1997). The errors of $\log v$ in units of 0.01 are shown in parentheses; they are compounded from the observational errors and the peculiar velocities, assumed to be 200 km s^{-1} within 1500 km s^{-1}, 400 km s^{-1} for 1500 < v < 3000 km s^{-1}, and 600 km s^{-1} beyond 3000 km s^{-1}. **(4)-(6)**: B-, V-, and I-band apparent peak magnitudes. They are in the Cerro Tololo system of fitting light curve templates (Hamuy et al. 1996b,c). The template fitting for the observations by Riess et al. (1999) was done by us. All magnitudes are corrected for Galactic absorption. Where applicable, the K-correction (Hamuy et al. 1993) was taken into account. The magnitude errors in units of $0\overset{m}{.}01$ were taken from the original literature or were estimated by us. **(7)**: The Galactic absorption A_V from Schlegel et al. (1998), assuming A_B=4.3 $E(B\text{-}V)$, A_V=3.3 $E(B\text{-}V)$, and A_I=2.0 $E(B\text{-}V)$ throughout. **(8)**: Δm_{15} being the decline in magnitudes of the B light curve during the first 15 days after maximum, as defined by Phillips (1993). The magnitude errors in units of $0\overset{m}{.}01$ were taken from the original literature or were estimated by us. **(9)**: The onset of the photometric data given in days before (minus signs) and after (plus signs) B maximum. **(10)**: References for the photometric data B, V, I and Δm_{15}. **(11)-(13)**: Absolute magnitudes at maximum as calculated from the apparent magnitudes in columns (4) to (6) and from the recession velocities in column (3). A flat matter universe (Ω_M=1) and a value of H_0 = 60 km s^{-1} Mpc^{-1} is assumed. As a consequence all listed absolute magnitudes scale, except for peculiar velocities, with 5 $\log(H_0/60)$. The errors in units of $0\overset{m}{.}01$ are compounded from the errors given in columns (3) and (4) to (6), respectively. No absolute magnitudes were calculated for SNe Ia in the field with v_{220} < 1200 km s^{-1} because their velocity distances are too unreliable due to peculiar motions, and for five SNe Ia in Virgo cluster galaxies because of the considerable cluster depth. For four SNe Ia of Table 1 independent absolute magnitudes from Cepheid distances are given in Table 3; they are marked with asterisks.

In the following the overluminous SN 1991 T (Phillips et al. 1992) and its twin SN 1995 ac (Garnavich et al. 1996) are left out because they are spectroscopically peculiar, leaving in Table 1 59 blue SNe with $(B\text{-}V)\leq 0.20$ and $v_{220} \geq$ 1200 km s^{-1}. The observations of six SNe Ia after 1985 in Table 1 begin only eight days after maximum or later. Their extrapolated maximum magnitudes may be less accurate (Phillips et al. 1999). In the diagrams to follow they are shown with small symbols, but they have no systematic effect on any of the conclusions below and are included in the equations below with their errors as given in Table 1. The I-observations of SN 1992 au begin only 15 days after B maximum and are not considered in the following.

In Table 2 data are compiled that are relevant for a localization of the SNe Ia of Table 1 within their host galaxies. Columns (1) to (6) are self-explanatory. The diameters D_{25} (in arcsec), given

in column (7) where available, are taken from the on-line Asiago Supernova Catalogue (Cappellaro 1998) and the RC3 (de Vaucouleurs et al. 1991). Columns (8) and (9) give the supernova offsets in the E/W and N/S directions as taken from Cappellaro (1998) and from Riess et al. (1999). The projected galactocentric distances of the SNe in units of the galaxy radius r_{25} ($=D_{25}/2$) are given in column (10); they are distance-independent.

2.2. The Cepheid-calibrated SNe Ia

Table 3 lists the nine SNe Ia for which Cepheid distances and therefore absolute magnitudes are known. The apparent or true distance moduli from Cepheids and their sources are given in columns (4) to (7). The moduli from the WFPC 2 are corrected by $+0^m\!.05$ for the photometric short exposure/long exposure zeropoint effect (Stetson 1995; Saha et al. 1996a). The apparent B, V, and I magnitudes at maximum (uncorrected for Galactic absorption) and their sources are in columns (8) to (11). The total color excesses E_{B-V} (Galactic and within the host galaxy) and their sources are listed in columns (12) to (13). The absorption-corrected apparent magnitudes B^0, V^0, and I^0 are given in columns (14) to (16). The absolute magnitudes M_B^0, M_V^0, and M_I^0 follow in columns (17) to (19). For the first four SNe Ia the absolute magnitudes are derived by subtracting the *apparent* distance moduli from the respective *apparent* magnitudes on the plausible assumption that the Cepheids and the corresponding SN Ia suffer the same (small) amount of absorption. In the remaining cases either the Cepheids have variable absorption or the SN suffers additional absorption in its host galaxy. In these cases the absolute magnitudes come from subtracting the *true* distance moduli from the *true* magnitudes. Finally, the decline rates Δm_{15} in column (20) are taken from the references in column (11). The straight and weighted mean absolute magnitudes of eight SNe Ia in Table 3 are given at the bottom of the Table. The bright SN 1895 B is not included because its V maximum is known too poorly. — The adopted absolute magnitudes are in fortuitous agreement with theoretical models of *blue* supernovae (Höflich, P., & Khokhlov 1996) and Branch's (1998) discussion of the physical properties of SNe Ia.

Five SNe in Table 3 are not included in Table 1. SN 1895 B has no reliable color information. SNe 1989 B and 1998 bu are observed to be much redder than (B-V)=0.20. SNe 1974 G and 1981 B are *known*, in spite of their rather blue color, to suffer reddening in their host galaxy.

The eight Cepheid distances adopted in Table 3 have been re-analysed by Gibson et al. (2000b) (hereafter G00). They have used ALLFRAME photometry and the associated method of detecting variable stars. They claim that this re-analysis places their galaxy distances on the same footing as the distances of galaxies contained in the Mould-Freedman-Kennicutt (MFK; e.g. Mould et al. 2000) program. However, this claim is questionable for several reasons:

(i) While the MFK team has consistently quoted photometry from ALLFRAME (though DoPHOT magnitudes have also been presented for comparison), their list of Cepheids comprised objects independently detected by both ALLFRAME *and* DoPHOT. The Sandage/Saha consor-

tium have based their Cepheid selection and photometry on DoPHOT alone. A salient result of the G00 re-analysis is that the agreement of the photometry of stars that are *in common* between them and the Sandage/Saha team must be excellent, because if one compares only the 118 Cepheids in common in six galaxies (as given in Table 3 of G00), the difference in the magnitudes averages to be ΔV=-0$^m_.$044$\pm$0$^m_.$002, ΔI=-0$^m_.$038$\pm$0$^m_.$004, in the sense that the ALLFRAME-based magnitudes are brighter. Thus if the procedure that was actually used to derive distances by the MFK team in their program is applied, the agreement between ALLFRAME- and DoPHOT-based magnitudes in V and I, and hence in moduli, is as good as one can expect, and the confidence in the DoPHOT-based results is bolstered.

However, G00 have added Cepheids found only by ALLFRAME. These "extra" Cepheids drive a distinctly different result, increasing the mean difference DoPHOT-moduli (of the Sandage/Saha team) minus ALLFRAME-moduli (of G00) to 0$^m_.$17. Had G00 reported results that are truly on the same footing as the rest of the MFK team analysis, they would not have seen the 0$^m_.$17 "discrepancy".

ii) G00 specially point out that in the case of NGC 4536 Saha's et al. (1996a) Cepheids in Chip 2 of the WFPC2 give a distance modulus that is larger by 0.66 mag, which is the result of differences in the photometry in V and/or I by order of 0.25 mag. G00 do not see this discrepancy in their own reduction: their photometry in all four chips are in mutual agreement, and also in nominal agreement with Saha's et al. (1996a) photometry in chips 1, 3, and 4. It is worth emphazising that the region of the galaxy imaged in chip 2 is different in character from that in chips 3 and 4 (chip 1 is similar to chip 2, but there are too few Cepheids to make a statistically significant difference): the latter are dominated by the outer spiral arms, but chip 2 shows the more amorphous inner regions. Such changes in environment can contribute different levels of confusion noise, and consequently result in mis-calibration of the zero-point. To be consistent with their work in other galaxies and having no external information on which chip is best, Saha et al. (1996a) have combined their Cepheids, as measured, in a single PL relation and have derived an average distance modulus, their rationale being that the exceptional chip-to-chip variation of NGC 4536 may just be the result of an unusually large *statistical* fluctuation. The point illustrates that the chip-to-chip variations of the aperture correction in crowded regions is the weakest link in WFPC2 photometry. Cepheid moduli from the WFPC2 therefore always carry an uncertainty of 0.10-0.15 mag. The error is random from galaxy to galaxy and is therefore reduced by a sufficient number of calibrators.

(iii) The analysis of G00 differs also from the present one in the way the reddening is handled, both of the Cepheids as well as of the SNe Ia. The G00 approach is to always de-redden the Cepheids, and then to obtain the de-reddened modulus to the host galaxy. This approach is unavoidable if the extinction of the Cepheids is much larger than that of the SN Ia (NGC 4639 with SN 1990 N), if the Cepheids have differential reddening (NGC 3627), or/and if the SNe Ia have large, but pre-determinded reddenings (SN 1974 G, 1981 B, 1989 B, and 1998 bu). Yet de-reddening procedures demand exquisite photometry, since the ratio of total to selective absorption amplifies the uncertainties in the photometry. Therefore, instead of going through the de-reddening twice

(once for the Cepheids and once for the SNe Ia), it is preferable to assume that the reddening of the Cepheids and of the SNe Ia is the same whenever the reddening is small ($\lesssim 0^m.03$). In that case the SN luminosity is obtained by simply subtracting the apparent distance modulus from the apparent SN magnitude. This procedure has been applied for the first four entries in Table 3.

After the reddening corrections of G00 are applied, the "discrepancy" of $0^m.17$ drops to $0^m.04$, $0^m.07$, and $0^m.15$, in M_B, M_V, and M_I, respectively. The consequence of this calibration then is — if applied to the fiducial sample — that the value of $H_0(I)$ becomes larger by five percent than $H_0(B)$ while with the present calibration in Table 3 the values of H_0 agree almost exactly in all three passbands (cf. Section 4).

Remaining systematic error sources, which may affect the calibrators, are discussed in Section 6.

3. The Colors of SNe Ia

3.1. Justification for the *blue* sample of SNe Ia

In Table 1 and in the following sections only SNe Ia with $(B\text{-}V)\leq 0^m.20$, called blue SNe Ia, are considered. This color cut needs justification. In Figure 1 *all* SNe Ia between 1985 and 1996 with known peak magnitudes are plotted, unrestricted as to color $(B\text{-}V)$. The restriction to SNe Ia after 1985 is here and in the following indicated because the advent of CCD photometry has much improved the photometric accuracy. The SNe Ia colors are only corrected for Galactic reddening. 44 SNe Ia are strongly concentrated toward a mean color of $(B\text{-}V)=0^m.02$ with a scatter of only $\sigma_{B-V}=0^m.05$. This small scatter is even the more surprising as Hamuy et al. (1996b, Table 6) list an average observational error in color of $0^m.06$. The *true* color scatter of this subsample could therefore be arbitrarily small. As far as spectra of this blue subsample are known they are all Branch-normal (Branch et al. 1993), the only exceptions being the twins SN 1991 T and 1995 ac with peculiar early specta. As mentioned before they are excluded in the following.

The 10 SNe Ia in Fig. 1 with $(B\text{-}V)>0^m.20$ contain a high fraction of spectroscopically peculiar objects, like the very red and strongly underluminous SN 1991 bg and the low-expansion velocity SN 1986 G and their counterparts, as well as some presumably strongly reddened SNe Ia. These red SNe Ia clearly form a very heterogeneous group.

It is obvious that if SNe Ia are to be used as standard candles, one must concentrate on the homogeneous class of *blue* SNe Ia.

3.2. The true colors of SNe Ia

Even the sample of 42 blue SNe Ia may be affected by some internal reddening. Their true colors are best reflected by SNe Ia that have occured in E/S0 galaxies or lie in the outer regions

of spirals. Outlying SNe Ia are here defined as having r/r_{25}>0.4, where r is the radial distance from the center of the host galaxy (in arcsec), and r_{25} is the de Vaucouleurs radius of that galaxy (in arcsec). The r/r_{25} values are listed in Table 4 for all SNe for which the necessary data are available. The relative radial distance r/r_{25}>0.4 corresponds roughly to the limit to which the spiral structure can be traced.

Table 4 lists the mean colors <B-V> and <V-I> of all SNe Ia in E/S0 galaxies, of the outlying SNe Ia in spirals, and of the calibrators in Table 2. The three groups have closely the same mean colors, i.e. <B-V>=-0.012±0.051 and <V-I>=-0.276±0.078. The overall means are therefore adopted as the true colors of SNe Ia in E/S0s and spirals alike.

Phillips et al. (1999) have instead derived the intrinsic colors by assuming that all SNe Ia with $E(B\text{-}V)_{Tail}$<0.06 are unreddened. (For their new method to derive $E(B\text{-}V)_{Tail}$ see the original paper). They give $E(B\text{-}V)$ and $E(V\text{-}I)$ values for 40 SNe Ia with B- and for 32 SNe Ia with I-magnitudes in their Table 1. If these color excesses are applied to the magnitudes in Table 1 one obtains mean colors of <B-V>=-0.051±0.007 and <V-I>=-0.331±0.013, i.e. noticeably bluer by $\sim 0^m_.04$ than adopted in Table 4. It seems therefore that the color excesses of Phillips et al. (1999) are too large. The difference is not trivial when converted to absorption, i.e. $A_B \approx 0.16$; it has, however, no effect on H_0 as long as the adopted colors of the calibrators and the distant SNe Ia are the same.

3.3. Blue, yet reddened SNe Ia

The question remains whether some of the SNe Ia in the inner regions of the spirals, i.e. $r/r_{25} < 0.4$, are affected by internal absorption. Figure 2 shows the correlation as to color (B-V) with radial distance for all SNe Ia for which the necessary data are available. There are five inner SNe Ia in spirals which are redder than (B-V)=$0^m_.06$. Since their absolute magnitudes are also fainter than average they are strong candidates for some internal absorption. They are listed in Table 5 together with two additional SNe Ia that fullfill the same color and magnitude requirement, but for which r/r_{25} is not available.

The colors (B-V) and (V-I) in columns 3 and 4 of Table 5 are from data in Table 1. These colors and the adopted mean color in Table 4 give the excesses $E(B\text{-}V)$ and $E(V\text{-}I)$. If these are averaged, giving double weight to the former and assuming $E(B\text{-}V)$=0.6 $E(V\text{-}I)$, one obtains the mean excesses $E(B\text{-}V)$ in column 5, which in turn lead to the absorption-corrected apparent (columns 6 to 8) and absolute (columns 9 to 11) magnitudes of the SNe Ia. They are on average close to the absolute magnitudes of the unreddened SNe Ia. Phillips et al. (1999) have given reddening values for four objects in Table 5; they are also above average. The strongest argument for the internal extinction is, however, that at given Δm_{15} they are fainter on average by $0^m_.38$ in B, $0^m_.30$ in V, and $0^m_.14$ in I than their unreddened counterparts (cf. below, Section 5.1). This magnitude difference practically disappears once the extinction corrections have been applied.

Because the seven SNe Ia of Table 5 being reddened cannot be proved beyond doubt, they are excluded henceforth. If they had been retained without absorption correction they would slightly decrease the value of H_0; if included after the absorption correction they would not have a net effect on H_0.

It is reassuring that the remaining 10 SNe Ia in spirals, which have $r/r_{25}<0.4$ or for which no information is available as to radial distance, have closely the same mean colors as the unreddened SNe Ia (Table 4).

4. The Hubble Diagram

After the exclusion of SNe 1991 T and 1995 ac, and the I-band magnitude of SN 1992 au, as well as the seven SNe Ia in Table 5, Table 1 contains 35 (29 of which have also I-magnitudes) blue, unreddened SNe Ia after 1985 and with v>1200 km s^{-1}. They are referred to in the following as the *fiducial sample*. Their Hubble diagrams in B, V, and I are shown in Fig. 3. Fitted to the data is a Hubble line assuming a flat Universe with Ω_M=0.3 and Ω_Λ=0.7 (for a justification of this choice cf. Section 6). In that case the Hubble line is described by (cf. Carroll, Press, & Turner 1992)

$$m_{B,V,I} = 5\log\left(\frac{c}{H_0}(1+z_1)\int_0^{z_1}[(1+z)^2(1+\Omega_M z)-z(2+z)\Omega_\Lambda]^{-1/2}dz\right)+M_{B,V,I}+25\,. \quad (1)$$

Inserting the weighted values $M_{B,V,I}$ of the calibrators from Table 3 the best fit to the data is achieved by weighted χ^2 solutions in B, V, and I. They give as a preliminary result a Hubble constant[5] of H_0(B)=58.3±1.1, H_0(V)=57.9±1.8, and H_0(I)=58.8±2.6, with a mean value of

$$H_0(BVI) \;=\; 58.3\pm2.0\,. \quad (2)$$

The scatter about the Hubble lines in Fig. 3 is σ_B=0.214, σ_V=0.181, and σ_I=0.161 mag, proving in favor of the use of SNe Ia as standard candles. The scatter is somewhat larger within v=10 000 km s^{-1} than beyond, which must be due to the influence of peculiar motions. The quoted values of σ are therefore upper limits of the intrinsic luminosity scatter.

5. The Correlation of SN Ia Luminosities with Second Parameters

Even the small scatter of $\sigma_B=0\overset{m}{.}21$ in the Hubble diagram of the fiducial sample spans a total range of SN Ia luminosities of $\sim0\overset{m}{.}6$. This is enough of a variation to ask whether their individual luminosities depend on second parameters. If that is the case one must make sure that the calibrators in Table 3 have the same mean second parameters as the SNe of the fiducial sample.

[5]In the remainder of this paper a value of the Hubble constant is always understood in terms of km s^{-1} Mpc^{-1}.

Even the SNe Ia with Branch-normal spectra (Branch et al. 1993) show some spectral variations which apparently correlate with the expansion velocity, the effective temperature — presumably a result of variable amounts of ^{56}Ni produced in the explosion —, *and* the peak luminosity (Nugent et al. (1995), cf. also Mazzali et al. (1998)). Attempts to homogenize all blue SNe Ia to a common mean spectrum and thus to make them even better standard candles are doomed, as stated before, because too few SNe Ia of the fiducial sample have the necessary spectral information.

As a consequence one has searched for purely empirical second parameters that correlate with the peak luminosity. The first success was the decline rate Δm_{15} of the B light curve, which measures the decline in magnitudes during the first 15 days after B maximum (Phillips 1993). Other second parameters followed like the SN light curve shape (Riess et al. 1996; Perlmutter 1998), the SN color (B-V) at B maximum (Tammann 1982; Tripp 1998), the color (Branch et al. 1996b) or the Hubble type (Hamuy et al. 1995; Saha et al. 1997, 1999) of the parent galaxy, or the position within the latter (Wang et al. 1997; Riess et al. 1999). There is a considerable literature on the subject.

The dependence of SNe Ia luminosities on second parameters is re-investigated here on the basis of an enlarged, well-defined sample.

5.1. Decline Rate Δm_{15}

The B, V, I residuals, read in magnitudes, from the Hubble line in Fig. 3, i.e. $\delta m = m_{obs} - m_{fit}$, are plotted versus the decline rate Δm_{15} in Fig. 4.

The clear dependence of SN luminosity on Δm_{15} is expressed by the following linear regressions (weighted by the errors in $M_{B,V,I}$ as given in Table 1, columns (11) to (13)):

$$\delta m_B^{15} = 0.48_{\pm 0.13}\,(\Delta m_{15} - 1.2) - 28.410_{\pm 0.161}, \quad \sigma = 0.194, \quad n = 35 \tag{3}$$

$$\delta m_V^{15} = 0.50_{\pm 0.11}\,(\Delta m_{15} - 1.2) - 28.394_{\pm 0.143}, \quad \sigma = 0.151, \quad n = 35 \tag{4}$$

$$\delta m_I^{15} = 0.39_{\pm 0.13}\,(\Delta m_{15} - 1.2) - 28.118_{\pm 0.171}, \quad \sigma = 0.144, \quad n = 29 \tag{5}$$

If the linear regressions are made by allowing for the errors both in m *and* Δm_{15} one finds somewhat steeper slopes. However, any steeper slope introduces a dependence of the luminosity on Δm_{15} of opposite sign (i.e. SNe Ia with large values of Δm_{15} become too bright). If errors both in m and Δm_{15} are considered one has to impose the additional condition that any dependence of absolute magnitude (or δm) on Δm_{15} vanishes. In this case one recovers equations (3) to (5). Some authors have also suggested steeper slopes by forcing a relation through all kinds of SNe Ia including the heterogenous set of red objects (cf. Section 3.1). Equations (3) to (5) apply explicitely only to SNe Ia which fullfill the conditions imposed on the fiducial sample. The decisive point is that these conditions (with the exception of recession velocity), i.e. reasonably good photometry in B and V, blue intrinsic colors (B-V), and Branch-normal spectra whereever known, are perfectly met also by

the calibrators, and hence they must comply with the same equations. (It may be noted in passing that the calibrators alone suggest an even somewhat shallower slope).

Correcting the SNe Ia magnitudes for Δm_{15} according to equations (3) to (5) has two effects: i) it reduces the scatter in m to the indicated values, and ii) it increases H_0 because the calibrators have somewhat smaller Δm_{15} on average than the fiducial sample (cf. Section 6 below).

5.2. SN color (B-V)

The rediduals $\delta m = m_{obs} - m_{fit}$ from the Hubble line in Fig. 3 are plotted versus SN color (B-V) in Fig. 5. Weighted linear regressions through the data in Fig. 5 give

$$\delta m_B^{\rm col} = 2.55_{\pm 0.46}\,[(B-V)+0.01] - 28.371_{\pm 0.027}, \quad \sigma = 0.160, \quad n = 35 \tag{6}$$

$$\delta m_V^{\rm col} = 1.50_{\pm 0.40}\,[(B-V)+0.01] - 28.348_{\pm 0.024}, \quad \sigma = 0.164, \quad n = 35 \tag{7}$$

$$\delta m_I^{\rm col} = 1.17_{\pm 0.43}\,[(B-V)+0.01] - 28.083_{\pm 0.029}, \quad \sigma = 0.148, \quad n = 29 \tag{8}$$

In spite of the considerable observational errors of (B-V) the dependence on luminosity is significant. In fact comparison of the luminosity scatter in equations (6) to (8) with the ones in equations (3) to (5) shows that (B-V) is as efficient as the decline rate Δm_{15} to reduce the scatter. This is in line with the conclusion of Tripp (1998). The dependence of the SN Ia luminosity on color must be mainly an *intrinsic* effect of SNe Ia (Tammann & Sandage 1995). The proposal that it is due to absorption in the parent galaxy (Riess et al. 1996) has been criticized before (Branch et al. 1996a; Saha et al. 1997). Indeed, if the Galactic absorption law applies on average, the coefficient of the color term in equations (6) to (8) would have to be ∼4, ∼3, and ∼2, respectively, which is excluded at the 3-4 sigma level. The decisive proof against absorption being the main source of the color variations is the fact that SNe Ia become *brighter* in I as their (V-I) colors become *redder* (Saha et al. 1999), which is here confirmed.

The color correction has no effect on H_0 derived below, because the calibrators and the fiducial sample have closely the same colors (cf. Table 4).

5.3. Combining decline rate Δm_{15} and color (B-V)

The colors (B-V) of the SNe Ia of the fiducial sample do not correlate with the decline rates Δm_{15}. These two parameters being orthogonal should hence be combined for an optimum homogenization of the blue SNe Ia. If the residuals $\delta m = m_{obs}$-m$_{fit}$ of the fiducial sample are fit simultaneously by a least-squares solution for two free parameters linear in Δm_{15} and (B-V) one obtains

$$\delta m_B^{\rm corr} = 0.44_{\pm 0.13}\,(\Delta m_{15} - 1.2) + 2.46_{\pm 0.46}\,[(B-V)+0.01] - 28.400_{\pm 0.161},\ \sigma_B = 0.129 \tag{9}$$

$$\delta m_V^{\rm corr} = 0.47_{\pm 0.11}\,(\Delta m_{15} - 1.2) + 1.39_{\pm 0.40}\,[(B-V) + 0.01] - 28.391_{\pm 0.143},\ \sigma_V = 0.129 \quad (10)$$

$$\delta m_I^{\rm corr} = 0.40_{\pm 0.13}\,(\Delta m_{15} - 1.2) + 1.21_{\pm 0.43}\,[(B-V) + 0.01] - 28.105_{\pm 0.171},\ \sigma_I = 0.122 \quad (11)$$

The coefficients are similar and their errors are equal to those appearing in equations (3) to (8). They are also in statistical agreement with those proposed by Tripp (1998) and Tripp & Branch (1999). A Fisher F-test for an additional term (Bevington & Robinson 1992) shows that the inclusion of a second parameter is significant at the 99.9 percent level. The scatter is now reduced to $\lesssim 0\overset{m}{.}13$ which is significantly less than from either Δm_{15} or (B-V) corrections alone. In fact the scatter is now of the same order as an (optimistic) estimate of the combined observational errors in m, Δm_{15}, and (B-V).

5.4. Hubble Type

A correlation between the SNe Ia luminosities and the color of the parent galaxy has been pointed out by Branch et al. (1996b). Instead of galaxy color we consider here, following Hamuy et al. (1995) and Saha et al. (1997, 1999), the Hubble type of the parent galaxy because many of them have known Hubble types but no colors.

The left panel of Fig. 6 shows the correlation of the residuals m_{obs}-m$_{fit}$ on the Hubble type T (from Table 1, column 2). A weighted least-squares fit gives for the V residuals, where the effect is most pronounced, m_{obs}-m$_{fit}\sim$(-0.017±0.013) T, which is only moderately significant. Taken at face value it implies that SNe Ia in E galaxies (T=-3) are on average fainter by ΔV=0.14±0.10 mag than their counterparts in Sc spirals (T=5). The type dependence is somewhat stronger for SNe Ia within 10 000 km s^{-1} and disappears at large distances; this can presently only be explained by invoking a statistical fluke. The luminosity dependence on the stellar population is presumably due to metallicity effects and/or different structures of the progenitor white dwarfs.

After homogenization of the fiducial sample as to decline rate Δm_{15} and color (B-V) according to equations (9) to (11) any significant dependence of the m^{corr}-m$_{fit}$ on T disappears. The reason is that there is a clear correlation of the decline rate Δm_{15} and the Hubble type. However, correcting the magnitude residuals by T instead of Δm_{15} is less effective, leaving a larger scatter about the Hubble line.

5.5. Galactocentric distance

In view of the dependence of SNe Ia luminosities on the Hubble type it is reasonable to ask whether the luminosities of SNe Ia depend on their distance $r_{\rm offset}$ from the center of their host galaxy, expressed in units ot the galaxy diameter r_{25}. The residuals m_{obs}-m$_{fit}$ are plotted versus the relative galactocentric distance $r_{\rm offset}/r_{25}$ in the left panel of Fig. 7 for all SNe Ia of the fiducial sample for which r_{25} is known. The interpretation of the formally significant fit of m_{obs}-

$m_{fit} \sim (0.27 \pm 0.11)\, r_{\rm offset}/r_{25}$, in all three colors, requires some caution because of the type mix and the uneven distribution in galactocentric distance. For spirals alone the effect is insignificant. Also the luminosity scatter does *not* significantly change with radial distance. This is in variance with Wang et al. (1997) and Riess et al. (1999) who suggested a larger luminosity scatter for the inner SNe Ia than for the outer ones. Their results depend heavily on the spectroscopically peculiar objects SN 1986 G, 1991 bg, and 1991 T, which happen to lie at small galactocentric distances; they are excluded here (cf. Section 2). Once the magnitude residuals are corrected for differences in decline rate and color through equations (9) to (11), the remaining slope of 0.11±0.08 (cf. Fig. 7, right panel) becomes even more marginal. Riess et al. (1999), discussing absolute galactocentric distances, came to the same conclusion. In any case the dependence of the luminosity on galactocentric distance has zero effect on the value of H_0 derived below.

6. The value of the Hubble constant

After correcting the magnitudes of the SNe Ia of the fiducial sample for differences in the decline rate Δm_{15} and the color (B-V) by means of equations (9) to (11), they define a Hubble diagram with a much reduced scatter, i.e. $\sigma_B \sim \sigma_V \sim \sigma_I \lesssim 0\overset{m}{.}13$ (Fig. 8). In fact the Hubble diagram is now so well defined that one may ask if a stand on a specific model Universe is required for relatively local SNe with $v \lesssim 30\,000\,{\rm km\,s^{-1}}$. The situation is visualized in a differential Hubble diagram (Fig. 9). Three different model Universes are fitted to the data:

1) A flat universe with $\Omega_M = 1.0$ (q_0=0.5; Sandage 1961, 1962). Taking the corresponding Hubble line and inserting the absolute magnitudes of the calibrators, corrected from equations (9) to (11) to be $M_B^{\rm corr}$=-19$\overset{m}{.}$48±0$\overset{m}{.}$07, $M_V^{\rm corr}$=-19$\overset{m}{.}$47±0$\overset{m}{.}$06, and $M_I^{\rm corr}$=-19$\overset{m}{.}$19±0$\overset{m}{.}$09, leads to a χ^2 solution with $\chi^2_{\nu,B}$=0.696 (σ_B=0$\overset{m}{.}$130) and H_0(B)=60.2±2.1. The values in V and I are very similar (60.1/60.0). The data give a somewhat better fit (at the $1\,\sigma$ level) on the assumption that H_0 is locally higher than the asymptotic value, i.e. H_0(v<10 000 km s^{-1})=60.8 (σ_B=0.137) and H_0(v>10 000 km s^{-1})=59.6 (σ_B=0.118) (Saha et al. 1999; Tammann et al. 1999). The difficulty with this solution is that the observational evidence speaks against a matter density as high as $\Omega_M = 1.0$ (for reviews cf., e.g., Bahcall 1997; Dekel et al. 1997; Tammann 1998).

2) An open Universe with $\Omega_M = 0.2$ (q_0=0.1; Sandage 1961, 1962). As compared to case 1) the χ^2_ν solution gives a better fit with $\chi^2_{\nu,B}$=0.633 (σ_B=0$\overset{m}{.}$124) and H_0(B)=60.3±2.0. The solutions for V and I are again very similar (60.2/60.1). The fit could still be improved with a smaller Ω_M, but Ω_M=0.2 is about as low as independent observations allow. The main difficulty here is, however, that the CMB fluctuations strongly suggest a flat universe with $\Omega_{\rm total}$=1.0 (Melchiorri et al. 1999; Macias-Perez et al. 2000).

3) A flat Universe with Ω_M=0.3, Ω_Λ=0.7 (q_0=-0.55). This is the model favored when including high-redshift SNe Ia out to $z \sim 0.8$ (Perlmutter 1998; Perlmutter et al. 1998, 1999; Riess et al. 1998b; Schmidt et al. 1998). The fit to the fiducial sample by means of equation (1) is with $\chi^2_{\nu,B}$=0.631,

$\chi^2_{\nu,V}$=0.802, $\chi^2_{\nu,I}$=0.589 (σ_B=$0\overset{m}{.}124$, σ_V=$0\overset{m}{.}123$, σ_I=$0\overset{m}{.}116$) somewhat better than with the two previous cases. However, an F-test shows that the improvement of the total χ^2_ν from three colors as compared to the case with Ω_M=1, H_0=constant, has a probability of not being a result of chance of only ∼70 percent. The corresponding values of the Hubble constant are $H_0(B)$=61.0±2.1, $H_0(V)$=60.9±1.8, and $H_0(I)$=60.7±2.6.

Not surprisingly, the specific choice of the cosmological model has only a minor effect on H_0. In all three cases H_0 lies within $60 < H_0 \leq 61$. Taking case 3) as the most consistent solution, a value of

$$H_0 \quad = \quad 60.9 \pm 4.0 \quad (2\,\sigma \ \text{error}) \tag{12}$$

is found. The errors account only for the statistical error of the absolute magnitude calibration (Table 3) and for the scatter about the Hubble line.

The solution in equation (12) is still affected by systematic errors. Sources of systematic errors and our estimate of their sizes are:

(1) The zeropoint of the DoPHOT photometry, on which six of the eight Cepheid distances in Table 3 are based, was independently checked by G00 as discussed in Section 2.2. They suggest that the DoPHOT magnitudes are too faint by $0\overset{m}{.}04$. On the other hand, a new zeropoint determination of the DoPHOT photometry shows that the previous zeropoint is still too bright by $0\overset{m}{.}02$ (Saha et al. 2000). Correspondingly, a zeropoint error of $\pm 0\overset{m}{.}04$ is allowed for.

G00 have proposed a total reduction of the distances of the Sandage/Saha team by $0\overset{m}{.}17$ on average. Yet it was shown in Section 2.2 that if G00 had used only those Cepheids found in common by both ALLFRAME and DoPHOT photometry (as appears to have been done for all the other galaxies studied by the MFK team) they would have obtained distances that are consistent within the statistical errors with those in Table 3. The smaller distances of G00 depend on the additional Cepheids found by ALLFRAME alone.

(2) Photometric blending of the Cepheids may lead to a systematic underestimate of the distances (Mochejska et al. 1999). Stanek & Udalski (1999) have proposed that the effect, increasing with distance, can amount to $0\overset{m}{.}3$ at 20 Mpc. Counter-arguments by Gibson et al. (2000a), also supported by Ferrarese et al. (2000), were judged to be weak (Paczyński & Pindor 2000). In general, it may be noted that the discovery mechanism for Cepheids favors large-amplitude Cepheids, while the amplitudes of blended Cepheids are reduced in function of the importance of the blend; moreover, many small-amplitude Cepheids have been excluded from our discussion because of their less convincing light curves. Indeed, a detailed analysis (Saha et al. 2000) of the effect in V and I of skewed error distributions from object confusion and surface brightness fluctuations reveals that the distance modulus of NGC 4639 has been underestimated by only $0\overset{m}{.}07$. This galaxy is the most distant one in Table 3, and the effect must be smaller for the others. An average distance modulus increase of $0\overset{m}{.}03 \pm 0\overset{m}{.}03$ seems reasonable.

(3) The adopted zeropoint of the Cepheid PL relation of $(m\text{-}M)_{\rm LMC}$=18.50 is likely to be too

small by $0\overset{m}{.}06\pm0\overset{m}{.}10$ (Federspiel et al. 1998; Gratton 1998; Madore & Freedman 1998; Feast 1999; Walker 1999; Gilmozzi & Panagia 1999). Smaller LMC moduli suggested on the basis of statistical parallaxes of RR Lyr stars and red-giant clump stars depend entirely on the sample selection and on the absence of metallicity and evolutionary effects, respectively. The higher LMC modulus will increase all moduli by $0\overset{m}{.}06\pm0\overset{m}{.}10$.

(4) The effect of metallicity variations on the Cepheid distances is a long-standing problem. Much progress has been made on the theoretical front. Saio & Gautschy (1998) and Baraffe et al. (1998) have evolved Cepheids through the different crossings of the instability strip and have investigated the pulsational behavior at any point. The resulting, highly metal-independent M(bol) have been transformed into PL relations at different wavelengths by means of detailed atmospheric models; the conclusion is that any metallicity dependence of the PL relations is nearly negligible (Sandage et al. 1998; Alibert et al. 1999). Bono et al. (1998) have suggested a much stronger metallicity dependence, but their conclusions depend entirely on the precarious treatment of convection at the red boundary of the instability strip.

From an observational point of view not even the sign of the metallicity effect on the luminosity is unanimously accepted. Based on [O/H] measurements the calibrating galaxies of Table 3 have a range of metallicities (Kennicutt et al. 1999). Allowing for this effect, G00 have suggested that their distances should be increased by $0\overset{m}{.}07$ on average. Kennicutt et al. (1998) and Feast (1999) recommend, on the other hand, that for the present no metallicity correction should be applied, but that for an uncertainty of $\gtrsim 0.1\,[\mathrm{Fe/H}]^{-1}$ (Feast 1999) should be allowed for. As a compromise it is adopted here that the distance moduli in Table 3 are underestimated by $0\overset{m}{.}04\pm0\overset{m}{.}10$ on average.

(5) There is the general trend of an incomplete Cepheid sampling near the photometry threshold to yield too short distances (Sandage 1988; Lanoix et al. 1999). According to Narasimha & Mazumdar (1998) and Mazumdar (1999) this effect has caused a distance underestimate of $\sim0\overset{m}{.}3$ in the extreme case of M100 (Ferrarese et al. 1996). This bias can be minimized by introducing a period cutoff, if the data allow so, at an appropriate low-period limit. Since the Cepheid moduli in Table 3 were derived in cognizance of the selection bias, the net effect on the luminosity calibration in Table 3 is most likely less than $0\overset{m}{.}1$. Here a systematic error of $0\overset{m}{.}05\pm0\overset{m}{.}05$ is allowed for.

(6) An overestimate of the absorption of the calibrating SNe Ia will lead to a spuriously low value of H_0, and vice versa. The opposite holds for over-corrected SNe Ia in the field. Yet a differential error of the extinction can be excluded at the level of $0\overset{m}{.}01$, because the calibrating SNe and those of the fiducial sample have nearly identical corrected colors (cf. Table 4). An error of the adopted *mean* color of SNe Ia has no effect on the distance scale because calibrating and field SNe Ia would be equally affected by the resulting change of the absorption. Concurrently the close agreement of H_0 from B, V, and I data speaks against hidden absorption problems. Absorption corrections can therefore not affect H_0 by more than $\pm$ 3 percent.

A ratio of $R_V{=}A_V/E(B\text{-}V){=}3.3$ was adopted here. With $R_V{=}3.0$ the calibrators would become fainter by $0\overset{m}{.}038$ on average, but the fiducial sample only by $0\overset{m}{.}014$. Therefore, while prefering

a value of R_V=3.3, a systematic uncertainty of the distances of $\pm 0\overset{m}{.}02$ should be allowed for.

It may be noticed that the nine SNe Ia of the fiducial sample with Galactic absorptions $A_V > 0\overset{m}{.}2$ have brighter absolute magnitudes M_B^{60} (Table 1) than their 26 counterparts with smaller Galactic absorption. The mean difference amounts to $0\overset{m}{.}21 \pm 0\overset{m}{.}04$ and is somewhat smaller in V and I, as is to be expected if the Galactic extinction corrections due to Schlegel et al. (1998) were somewhat too large for large values. If the nine strongly corrected SNe Ia are excluded, the Hubble line in Fig. 3 shifts faintwards by $0\overset{m}{.}05 \pm 0\overset{m}{.}04$, and H_0 is reduced by 2 percent. Furthermore the scatter in Fig. 8 shrinks to σ_B=0.114.

Finally, if the seven somewhat red SNe Ia in Table 5, which were excluded here on the assumption of internal absorption, were intrinsically red and hence included in the present analysis, they would slightly affect equations (9) to (11) and decrease H_0 by one percent. If they had been included after corrections for absorption, they would increase H_0 by much less than one percent.

(7) The coefficients of the Δm_{15}-term in equations (9) to (11) carry a random error of ± 0.13. This is to be multiplied with the mean difference $<\Delta m_{15}>$(fiducial sample)$-<\Delta m_{15}>$(calibrators)=0.17 to give a systematic error of the distances of $\pm 0\overset{m}{.}02$.

Phillips et al. (1999) have pointed out that the decline rate Δm_{15} is slightly affected by absorption. If this effect had been applied, the differential decline rate between calibrators and field SNe Ia would be changed by $\delta\Delta m_{15} = 0.008$ with vanishingly small effect on H_0.

(8) The redshift velocities were corrected for the CMB dipole motion on the assumption that the co-moving volume extends to 3000 km s^{-1}. If instead the volume size was varied between 2000 and 10 000 km s^{-1}, it would affect H_0 by less than one percent, as stated in Section 2.1. G00 have considered a very specific local flow model and concluded that in this case H_0 would be increased by two percent. This is taken as indication that the deviations from pure Hubble flow could influence H_0 by hardly more than $\pm\,2$ percent.

Most of the systematic errors, which are assumed to give 90-percent margins, tend to increase the true distance scale. If they are added linearly, H_0 in equation (12) would be reduced by a factor (0.91±0.07); if they are added in quadrature, instead, the reduction factor becomes (0.96±0.08). Multiplying the latter with equation (12) gives

$$H_0 \;=\; 58.5 \pm 6.3 \quad (2\,\sigma \text{ error}), \tag{13}$$

which is finally taken as our most probable value of the Hubble constant as inferred from Cepheid-calibrated SNe Ia, including random and systematic errors.

7. Alternative solutions

The second-parameter problem in finding H_0 could be avoided altogether, if the distant SNe Ia and the local calibrators had (nearly) identical second parameters. This can be approximated

by choosing a suitable subset of the fiducial sample. Excluding the 14 SNe Ia of the fiducial sample with the largest Δm_{15} values ($\Delta m_{15} \geq 1.3$), one is left with a rest sample of 21 objects with $<\Delta m_{15}>=1.08\pm0.02$, i.e. the same as for the calibrators.

Fitting the 21 (uncorrected) SNe Ia to equation (1) by a χ^2 solution and inserting the weighted absolute magnitudes of the calibrators in Table 3 gives $H_0(B)$=58.8, $H_0(V)$=58.8, and $H_0(I)$=59.9. This solution is not yet fully satisfactory, because on average the calibrators are now redder by $\Delta(B_0 - V_0) = 0.030 \pm 0.018$ and the Hubble type of their parent galaxies is still later by $\Delta T = 2.9\pm$ 0.7. But it should be noted that the result is rather close to the corresponding, fully corrected value of H_0=60.9 in equation (12).
As the sample of known blue SNe Ia with $v \lesssim 30\,000$ km s^{-1} will increase, this alternative solution will become more rigorously applicable and circumvent all corrections for second parameters.

Another alternative solution is given by confining the analysis to SNe Ia in spirals. Seven of the eight adopted calibrators lie in spirals. The population assignment of SN 1972 E is ambiguous because its parent galaxy is of Hubble type Am; the inclusion here of SN 1972 E does not affect the result. Nineteen of the SNe Ia of the fiducial sample after 1985 are in spirals ($T \geq 0$). Combining them with the calibrators and fitting them to equation (1) yields $H_0(B)$=59.0, $H_0(V)$=59.1, and $H_0(I)$=59.1. The spirals-only solution is remarkable because the mean solution of H_0=59.1 is smaller by only 3 % than the solution fully corrected for Δm_{15} and (B_0-V_0) in equation (12).

Thus both the exclusion of fastest-declining SNe and the restriction to only SNe in spirals provide useful simple approximations for the determination of H_0.

8. Conclusions

A fiducial sample of 35 well observed, blue (Branch-normal) SNe Ia with minimum absorption in their parent galaxies and with $1200 < v \lesssim 30\,000$ km s^{-1} has been compiled from the literature. For 29 SNe Ia also I-magnitudes are known. The intrinsic color of SNe Ia is found to be (B-V)=-$0\overset{m}{.}012\pm0.008$, ($V$-$I$)=-0.276±0.016 from objects in E/S0 galaxies and outlyers in spirals; the scatter in color of $\sigma=0\overset{m}{.}05$ for individual objects is surprisingly small.

The fit of the SNe Ia sample, although quite local ($z \lesssim 0.1$), to a Hubble line is somewhat dependent on the cosmological model adopted. Among various models, the marginally best fit is obtained for a flat Universe with Ω_M=0.3, Ω_Λ=0.7, which is presently also favored by external data. In this case the scatter about the Hubble line is $\sigma=0\overset{m}{.}21$-$0\overset{m}{.}16$, depending on the pass band. But the magnitude residuals correlate with decline rate Δm_{15} and color (B-V). If the dependency on either of these parameters is removed, the scatter is reduced to $\sigma=0\overset{m}{.}19$-$0\overset{m}{.}14$. A simultaneous correction for Δm_{15} and color (B-V) decreases the scatter to $\sigma \lesssim 0\overset{m}{.}13$ in all three colors. This illustrates the unique potential of SNe Ia as distance indicators.

If the SNe Ia of the fiducial sample are assigned the absolute magnitudes M_B, M_V, and M_I

of eight local SNe Ia whose Cepheid distances are known, one obtains closely the same value of H_0=58.3±2.0 for the three passbands. This solution is remarkably robust against various assumptions and corrections. Bootstrapping the calibrators by excluding two or three objects, does not change their mean absolute magnitude. The eight calibrators lie essentially all in spirals and they have correspondingly a somewhat smaller average Δm_{15} than the fiducial sample. If they are adjusted to the latter's mean Δm_{15}, H_0 is increased by 4 percent to H_0=60.9±2.0. A correction for (B-V) does not change this value because the calibrators and the fiducial sample have closely the same mean color. Any remaining dependencies on Hubble type and galactocentric distance are insignificant and have no effect on H_0. Alternative solutions considering either SNe Ia only in spirals or SNe Ia with small Δm_{15} — making the sample more similar to the calibrators — yields H_0≈59. The effect of systematic errors is mainly one-sided (photometric zeropoint, skewness of photometric errors, the LMC zeropoint of the PL relation, selection effects of Cepheids, and possibly metallicity effects), leading to too high values of H_0. If they are taken into account one obtains at the 90 percent confidence level H_0=58.5±6.3.

External results on H_0 from SNe Ia should be compared with H_0=60.9±2.0 from equation (12), because the subsequent corrections for systematic errors have not been applied yet in other papers. The results of Saha et al. (1999) and Tripp (1998) are indistinguishable from the above result despite of the re-definition of the "fiducial sample" here, of variations of other input data, and of independent corrections for Δm_{15} and (B-V). The value of H_0=62(±2) derived by Tripp & Branch (1999) from a sample of six calibrators and 13 field SNe Ia in spirals and fully corrected for Δm_{15} and (B-V) is in satisfactory statistical agreement with equation (12), too.

The somewhat higher value of H_0=63.9±2.2 by Suntzeff et al. (1999), based on only five of the calibrators in Table 3, is fully explained by their adopted steeper luminosity dependence on Δm_{15}, which is closely the same as was derived by Phillips et al. (1999), who included spectroscopically peculiar SNe Ia like SN 1986 G, 1991 T, 1991 bg, and 1995 ac. Had Suntzeff's et al. (1999) Δm_{15}-correction been applied to our fiducial sample, we would have obtained H_0=59.7 for the SNe Ia with Δm_{15}<1.2 (n=17), and H_0=64.6 for the ones with Δm_{15}≥1.2 (n=18). Since seven of the eight calibrators fall into the first category the lower value of H_0 is more nearly correct. The 3-σ discrepancy demonstrates that their Δm_{15}-correction introduces an over-correction, making the calibrators with a small mean Δm_{15} too faint and the field SNe Ia with large Δm_{15} too bright. This is the price to be paid if one attempts to derive a global correction formula which encompasses also peculiar objects that are extraneous of the SNe Ia sample to which it should be applied. — G00 have followed closely the line of Suntzeff et al. (1999), but they have reduced in addition the mean absolute magnitude of the calibrators by $\sim 0\overset{m}{.}2$ on the basis of quite objectionable additional Cepheids (cf. Section 2.2); their high value of H_0=68 (based on six calibrators) then follows by necessity. The repetition of one or two calibrating galaxies with the forthcoming Advanced Camera System on HST will bring a definitive decision on the merits of the additional Cepheids of G00, which were rejected here because their photometry relies so far only on ALLFRAME.

Jha et al. (1999) have derived H_0=64.4±5.4 from a sample of 42 distant SNe Ia and only four

Cepheid-calibrated SNe Ia. Seven of these objects have not been used here as either being too red or having peculiar spectra (SN 1992 K, 1995 ac). The SNe Ia are standardized by a "multi-color light curve shape" (MCLS) method giving simultaneously the absorption and a light-curve parameter substituting Δm_{15} (Riess et al. 1996, 1998b). Unfortunately the individual data are not given, and the discussion is restricted to V magnitudes denying a control on the consistency of colors. In spite of this, there is some question as to the grip of the MLCS light-curve parameter. The calibrators as well as the distant SNe Ia have still a magnitude scatter of $\sigma_V = 0\overset{m}{.}16$ after the correction, which is larger than $\sigma = 0\overset{m}{.}14$ obtained by Phillips et al. (1999) and significantly larger than $\sigma_V \leq 0\overset{m}{.}13$ found here by means of the corrections due to equation (10).

This discussion confirms previous investigations suggesting that if one attempts to derive H_0 from SNe Ia to within $\lesssim$10 percent, a major stumbling block are the second-parameter corrections. If the relatively mild Δm_{15}-corrections found here can be agreed upon it is clear that H_0 will settle close to 60 with a tendency for a small downward correction due to various (small) systematic errors.

Future Branch-normal SNe Ia in the field, preferably with $v \gtrsim 3000\,\mathrm{km\,s^{-1}}$, will help to settle the problem of light-curve shape corrections. The importance of these corrections will decrease as it will become possible to define sufficiently large sub-samples of field SNe Ia which have the same mean second parameters as the calibrating SNe Ia. Additional field SNe Ia are forthcoming (Nugent & Aldering 1999). Finally, the advent of the new Advanced Camera System on HST will allow to check the present Cepheid distances and to increase the number of calibrating SNe Ia.

At present the evidence from SNe Ia is best reflected at the 90-percent confidence level by a value of the Hubble constant, including random and systematic errors, of $H_0 = 58.5 \pm 6.3$.

We are grateful to B. Leibundgut for sharing some template-fitting software, M. Hamuy for providing us with a set of I band K-corrections, and B. Reindl for useful discussions. G.A.T. has profited from a Workshop on Supernovae (June 1999) at the Aspen Center for Physics. B.R.P. and G.A.T. acknowledge financial support of the Swiss National Science Foundation.

REFERENCES

Alibert, Y., Baraffe, I., Hauschildt, P., & Allard, F. 1999, A&A, 344, 551

Bahcall, N. 1997, in Critical Dialogues in Cosmology, ed. N. Turok, (Singapore: World Scientific), 221

Baraffe, I., Alibert, Y., Méra, D., Chabrier, G., & Beaulieu, J.-P. 1998, ApJ, 499, L205

Bevington, P.R., & Robinson, D.K. 1992, Data Reduction and Error Analysis for the Physical Sciences, 2nd ed. (New York: McGraw Hill)

Binggeli, B., Popescu, C., & Tammann, G. A. 1993, A&AS, 98, 275

Bono, G., Marconi, M., & Stellingwerf, R. F. 1998, ApJS, 122, 167

Branch, D. 1998, ARA&A, 36, 17

Branch, D., Fisher, A., & Nugent, P. 1993, AJ, 106, 2383

Branch, D., Fisher, A., Nugent, P., & Baron, E. 1996, in The Extragalactic Distance Scale, Poster Papers, eds. M. Livio, M. Donahue, & N. Panagia, (Baltimore: Space Telescope Science Institute), 4

Branch, D., Romanishin, W., & Baron, E. 1996, ApJ, 456, 73

Cappellaro, E. 1998, The Asiago Supernova Catalogue, http://athena.pd.astro.it/∼supern

Carroll, S. M., Press, W. H., & Turner, E. L. 1992, ARAA, 30, 499

Dekel, A., Burstein, D., & White, S. D. M. 1997, in Critical Dialogues in Cosmology, ed. N. Turok, (Singapore: World Scientific), 175

de Vaucouleurs, G. 1974, in The Formation and Dynamics of Galaxies, I.A.U. Symp. 58, 1

de Vaucouleurs, G., et al. 1991, Third Catalogue of Bright Galaxies, (New York: Springer), (RC3)

Feast, M. 1999, PASP, 111, 775

Federspiel, M., Tammann, G. A., & Sandage, A. 1998, ApJ, 495, 115

Ferguson, H.C. & Sandage, A. 1988, AJ, 96, 1520

Ferrarese, L., et al. 1996, ApJ, 464, 568

Ferrarese, L., et al. 2000, PASP, 112, 177

Fisher, A., Branch, D., Hatano, K., & Baron, E. 1999, MNRAS, 304, 67

Fisher, A., Branch, D., Höflich, P., & Khokhlov, A. 1995, ApJ, 447, L73

Garnavich, P. M., Riess, A. G., Kirshner, R. P., Challis, P., & Wagner, R. M. 1996, AAS, 189, #45.09

Gibson, B. K, Maloney, P.R., & Sakai, S. 2000, ApJ, 530, L5

Gibson, B. K, et al. 2000, ApJ, ApJ, 529, 723 [G00]

Gilmozzi, R., & Panagia, N. 1999, Space Telescope Science Institute Preprint Series, No. 1319

Gratton, R. 1998, in Abstracts of the 19th Texas Symposium on Relativistic Astrophysics and Cosmology, eds. J. Paul, T. Montmerle, and E. Aubourg, (CEA Saclay), 137

Hamuy, M., Phillips, M. M., Maza, J., Suntzeff, N. B., Schommer, R. A., & Avilés, R. 1995, AJ, 109, 1

Hamuy, M., Phillips, M. M., Maza, J., Wischnjewsky, M., Uomoto, A., Landolt, A. U., & Khatwani, R. 1991, AJ, 102, 208

Hamuy, M., Phillips, M. M., Suntzeff, N. B., Schommer, R. A., Maza, J., & Avilés, R. 1996a, AJ, 112, 2398

Hamuy, M., Phillips, M. M., Wells, L. A., & Maza, J. 1993, PASP, 105, 787

Hamuy, M., et al. 1996b, AJ, 112, 2408

Hamuy, M., et al. 1996c, AJ, 112, 2438

Höflich, P., & Khokhlov, A. 1996, ApJ, 457, 500

Jerjen, H. & Tammann, G. A. 1993, A&A, 276, 1

Jha et al. 1999, ApJS, 125, 73

Kennicutt, R. C., et al. 1998, ApJ, 498, 181

Kennicutt, R. C., et al. 1999, cited by Gibson et al. 2000

Kraan-Korteweg, R. 1986, A&AS, 66, 255

Lanoix, P., Paturel, G., & Garnier, R. 1999, ApJ, 517, 188

Leibundgut, B., et al. 1991a, ApJ, 371, L23

Leibundgut B., Tammann G. A., Cadonau R., & Cerrito D. 1991b, A&AS, 89, 537

Lira, P., et al. 1998, AJ, 115, 234

Macias-Perez, J.F., Helbig, P., Quast, R., Wilkinson, A., & Davies, R.D. 2000, A&A, 353, 419

Madore, B., & Freedman, W.L. 1998, ApJ, 492, 110

Mazumdar, A. 1999, in The Impact of Large-Scale Surveys on Pulsating Star Research, I.A.U. Coll. 176, in press

Mazzali, P.A., Cappellaro, E., Danziger, I.J., Turatto, M., & Benetti, S. 1998, ApJ, 499, L49

Melchiorri, A., et al. 1999, astro-ph/9911445

Mochejska, B.J., Macri, L.M., Sasselov, D.D., & Stanek, K.Z. 1999, AJ, submitted, astro-ph/9908293

Mould, J.R., et al. 2000, ApJ, 529, 786

Narasimha, D., & Mazumdar, A. 1998, astro-ph/9803195

Nugent P., & Aldering, G. 1999, in The Greatest Explosions Since the Big Bang: Supernovae and Gamma-Ray Bursts, Poster Papers, eds. M. Livio, N. Panagia, & K. Sahu, (Baltimore: Space Telescope Science Institute), 47

Nugent, P., Phillips, M., Baron, E., Branch, D., & Hauschildt, P. 1995, ApJ, 455, L147

Paczyński, B., & Pindor, B. 2000, astro-ph/0001417

Patat, F., Barbon, R., Cappellaro, E., & Turatto, M. 1997, A&A, 317, 423

Patat, F., Benetti, S., Cappellaro, E., Danziger, I.J., Della Valle, M., Mazzali, P.A., & Turatto, M. 1996, MNRAS, 278, 111

Perlmutter, S. 1998, in Supernovae and Cosmology, eds. L. Labhardt, B. Binggeli, & R. Buser, (Basel: Astronomisches Institut der Universität Basel), 75

Perlmutter, S., et al. 1998, Nature, 391, 51

Perlmutter, S. et al. 1999, ApJ, 517, 565

Phillips, M.M. 1993, ApJ, 413, L105

Phillips, M.M., Lira, P., Suntzeff, N.B., Schommer, R.A., Hamuy, M., & Maza, J. 1999, AJ, 118, 1766

Phillips, M.M. et al. 1992, AJ, 103, 1632

Richmond, M.W., et al. 1995, ApJ, 109, 2121

Riess, A.G., Nugent, P.E., Filippenko, A.V., Kirshner, R.P., & Perlmutter, S. 1998a, ApJ, 504,935

Riess, A.G., Press, W.H., & Kirshner, R.P. 1996, ApJ, 473, 88

Riess, A.G., et al. 1998b, AJ, 116, 1009

Riess, A.G., et al. 1999, AJ, 117, 707

Sadakane, K., et al. 1996, PASJ, 48, 51

Saha, A., Labhardt, L., & Prosser, Ch. 2000, PASP, 112, 163

Saha, A., Labhardt, L., Schwengeler, H., Macchetto, F. D. Panagia, N., Sandage, A., & Tammann, G. A. 1994, ApJ, 425, 14

Saha, A., Sandage, A., Labhardt, L., Schwengeler, H., Tammann, G. A., Panagia, N., & Macchetto, F. D. 1995, ApJ, 438, 8

Saha, A., Sandage, A., Labhardt, L., Tammann, G. A., Macchetto, F. D., & Panagia, N. 1996a, ApJ, 466, 55

Saha, A., Sandage, A., Labhardt, L., Tammann, G. A., Macchetto, F. D., & Panagia, N. 1996b, ApJS, 107, 693

Saha, A., Sandage, A., Labhardt, L., Tammann, G. A., Macchetto, F. D., & Panagia, N. 1997, ApJ, 486, 1

Saha, A., Sandage, A., Tammann, G. A., Labhardt, L., Macchetto, F. D., & Panagia, N. 1999, ApJ, 522, 802

Saio, H., & Gautschy, A. 1998, ApJ, 498, 360

Sandage, A. 1961, ApJ, 133, 355

Sandage, A. 1962, ApJ, 136, 319

Sandage, A. 1988, PASP, 100, 935

Sandage, A., Bell, R. A., & Tripicco, M. J. 1998, ApJ, 522, 250

Sandage, A., Saha, A., Tammann, G. A., Panagia, N., & Macchetto, F. D. 1992, ApJ, 401, L7

Schaefer, B.E. 1995, ApJ, 450, L5

Schaefer, B.E. 1998, ApJ, 509, 80

Schlegel, D., Finkbeiner, D.,& Davis, M. 1998, ApJ, 500, 525

Schmidt, B. et al. 1998, ApJ, 507, 46

Smoot G. et al. 1992, ApJ 396, L1

Stanek, K.Z., & Udalski, A. 1999, astro-ph/9909346

Stetson, P.B. 1995, private communication

Suntzeff, N.B., et al. 1999, AJ, 117, 1175

Tammann, G. A. 1982, in Supernovae: A Survey of Current Research, eds. M. J. Rees & R. J. Stoneham (Dordrecht: Reidel), 371

Tammann, G. A. 1998, in Primordial Nuclei and Their Galactic Evolution, eds. N. Prantzos, M. Tosi, R. von Steiger, (Dordrecht: Kluwer), 15

Tammann, G. A. & Federspiel, M. 1997, in The Extragalactic Distance Scale, eds. M. Livio, M. Donahue, & N. Panagia, (Cambridge: Cambridge University Press), 137

Tammann, G. A., Parodi, B. R., & Reindl, B. 1999, in The Impact of Large-Scale Structure on Pulsating Star Research, I.A.U. Coll. No. 176, in press (astro-ph/9911296)

Tammann, G. A., & Sandage, A. 1995, ApJ, 452, 16

Tanvir, N.R., Shanks, T., Ferguson, H.C., Robinson, D.R.T. 1995, Nature, 377, 27

Tripp, R. 1998, A&A, 331, 815

Tripp, R., & Branch, D. 1999, ApJ, 525, 209

Turner, A., et al. 1998, ApJ, 505, 207

Vaughan, T. E., Branch, D., Miller, D. L., & Perlmutter, S. 1995, ApJ, 439, 558

Walker, A. R. 1999, in Post-Hipparcos Cosmic Candles, eds. A. Heck & F. Caputo, (Dordrecht: Kluwer), 125

Wang, L., Höflich, P., & Wheeler, J. C. 1997, ApJ, 483, L29

Wells, L. A., et al. 1994, AJ, 108, 2233

Wu, H., Yan, H.-J., & Zou, Z.-L. 1995, A&A, 294, L9

Yahil, A., Tammann, G. A., & Sandage, A. 1977, ApJ, 217, 309

Fig. 1.— The color distribution of all known SNe Ia after 1985 with v$\lesssim$30 000 km s^{-1}. Open symbols are for SNe Ia with v<10 000 km s^{-1}, closed symbols are for more distant SNe Ia. The binned intervals embrace Δ(B-V)=$0\overset{m}{.}05$. A Gaussian fit to all SNe Ia with (B-V)$\leq 0\overset{m}{.}10$ gives <B-V>=0.020, σ_{B-V}=0.053.

Fig. 2.— Blue SNe Ia after 1985 plotted against the relative radial distance r/r$_{25}$. Circles stand for spiral, squares for E/S0 host galaxies. Small symbols represent SNe Ia with observations starting eight days after B maximum or later. Triangles are the calibrators from Table 3.

Fig. 3.— The Hubble diagrams in B, V, and I for the fiducial sample. Circles are SNe Ia in spirals, squares in E/S0 galaxies. Small symbols are SNe Ia whose observations begin eight days after B maximum or later. Solid lines are fits to the data assuming a flat universe with Ω_M=0.3 and Ω_Λ=0.7; dashed lines are linear fits with a forced slope of 0.2 (corresponding approximately to Ω_M=1.0 and Ω_Λ=0.0.). Not considered for the fits are the diamonds and the crosses representing SNe Ia dereddened according to Table 5 or observed before 1985, respectively.

Fig. 4.— Relative absolute magnitudes (i.e. residuals from the Hubble line in Fig. 3) for the SNe Ia of the fiducial sample in function of the decline rate Δm_{15}. Circles are SNe Ia in spirals, squares in E/S0 galaxies. Open symbols are SNe Ia with 1200 < v < 10 000 km s^{-1}, closed symbols are for the more distant SNe Ia. Small symbols are SNe Ia whose observations begin eight days after B maximum or later. Neither the SNe Ia before 1985 with known Δm_{15} (shown as crosses) nor the seven blue, but reddened SNe Ia (shown as X's) are considered for the weighted least-squares solutions (solid lines).

Fig. 5.— Relative absolute magnitudes (i.e. residuals from the Hubble line in Fig. 3) for the SNe Ia of the fiducial sample in function of their color (B-V). Symbols as in Fig. 4. Neither the few SNe Ia before 1985 (shown as crosses) nor the seven blue, but reddened SNe Ia (shown as X's) are considered for the weighted least-squares solutions (solid lines).

Fig. 6.— Relative absolute magnitudes (i.e. residuals from the Hubble line in Fig. 3) for the SNe Ia of the fiducial sample in function of their Hubble type T. Symbols as in Fig. 4. Left panel: m_{obs}-m_{fit}. Right panel: m^{corr}-m_{fit}, i.e. after magnitude corrections according to equations (9) to (11).

Fig. 7.— Relative absolute magnitudes (i.e. residuals from the Hubble line in Fig. 3) for the SNe Ia of the fiducial sample in function of their projected galactocentric distances r/r_{25}. Symbols as in Fig. 4. Left panel: m_{obs}-m_{fit}. Right panel: m^{corr}-m_{fit}, i.e. after magnitude corrections according to equations (9) to (11).

Fig. 8.— The Hubble diagrams in B, V, and I for the 35 (29) SNe Ia of the fiducial sample with magnitudes m^{corr} (i.e. corrected according to equations (11) to (13)). Symbols as in Fig. 3. The solid line is for a model with Ω_M=0.3, Ω_Λ=0.7, the dashed line for Ω_M=1.0, Ω_Λ=0.0.

Fig. 9.— Differential Hubble diagrams (m^{corr}-m_{fit}) vs $\log v$ in B, V, and I for the 35 (29) SNe of the fiducial sample. Symbols as in Fig. 3. The dashed line is for a flat cosmological model with Ω_M=1.0, Ω_Λ=0.0; the theoretical apparent magnitudes m_{fit} correspond to this model. The full line is for a flat model with Ω_M=0.3, Ω_Λ=0.7; the dotted line is for an open universe with Ω_M=0.2, Ω_Λ=0.0.

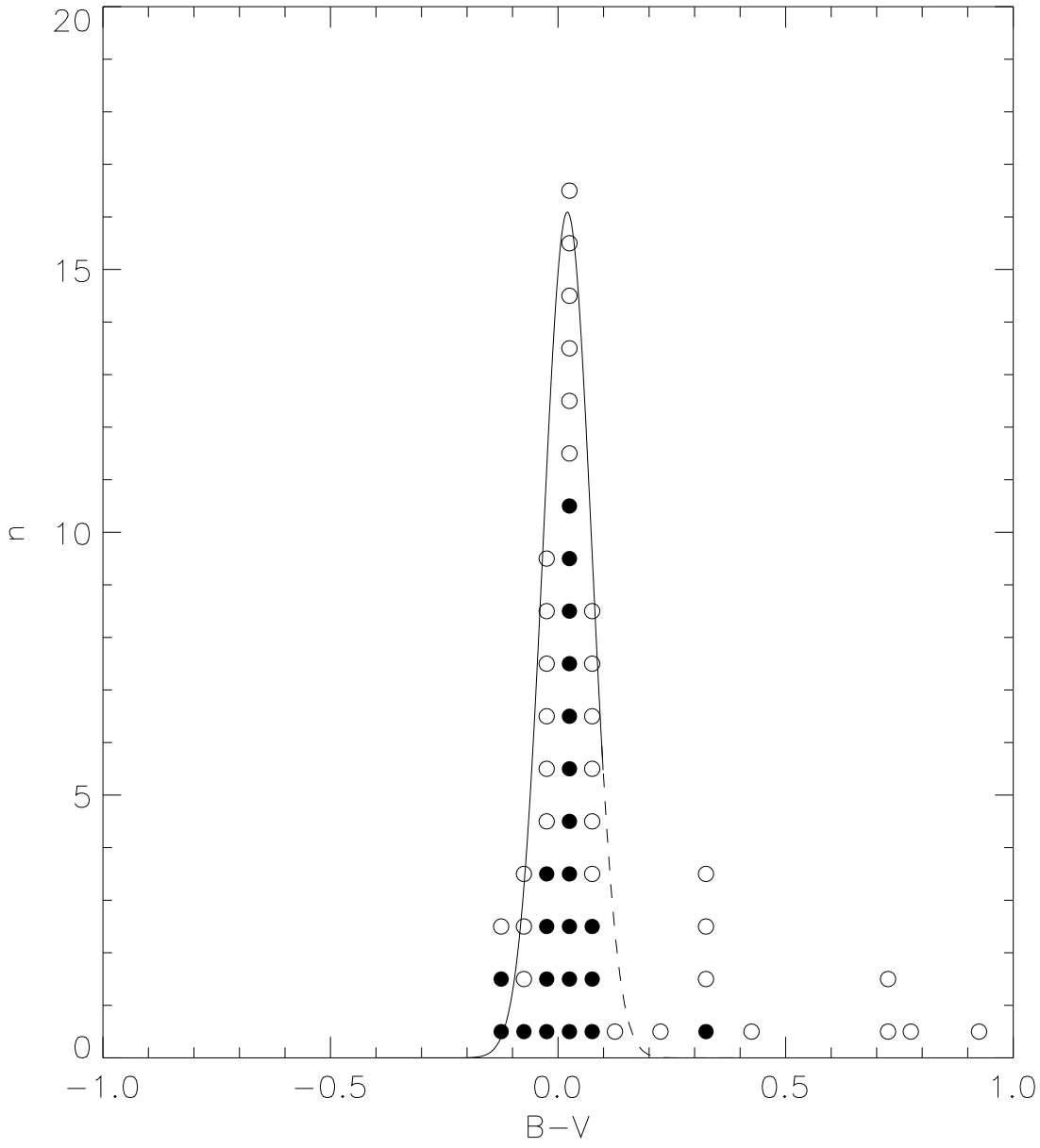

fig.1

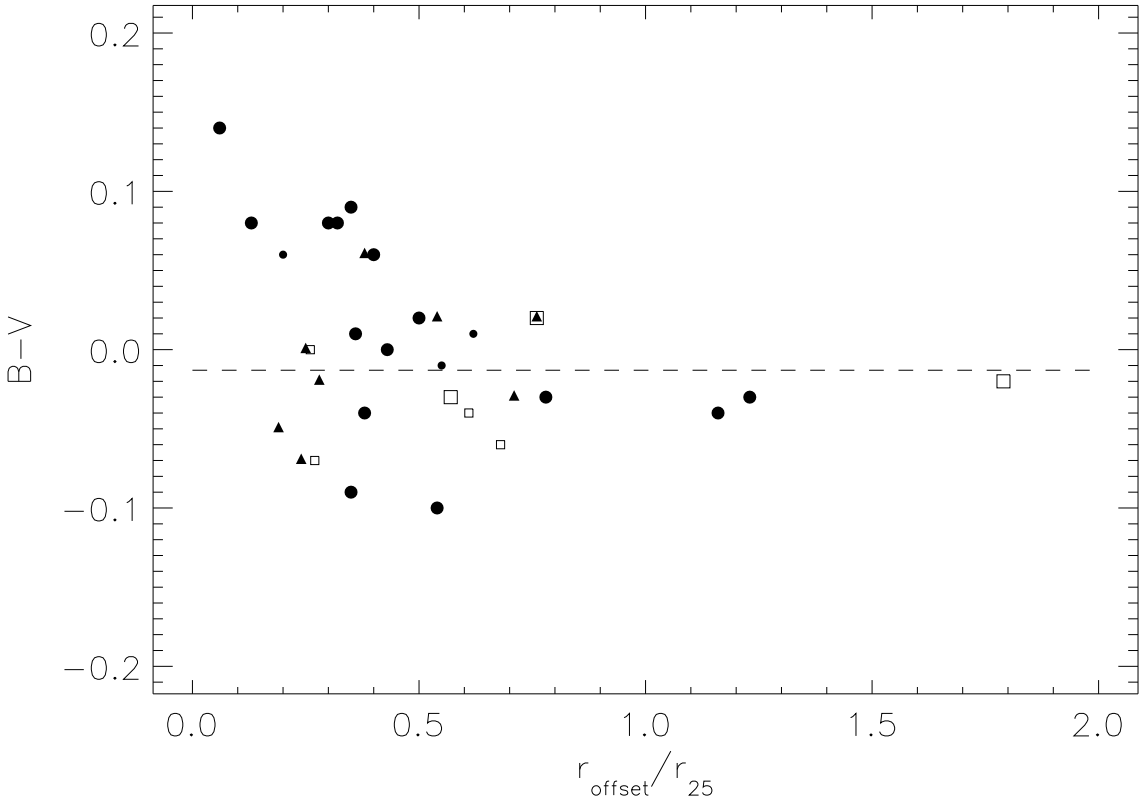

fig.2

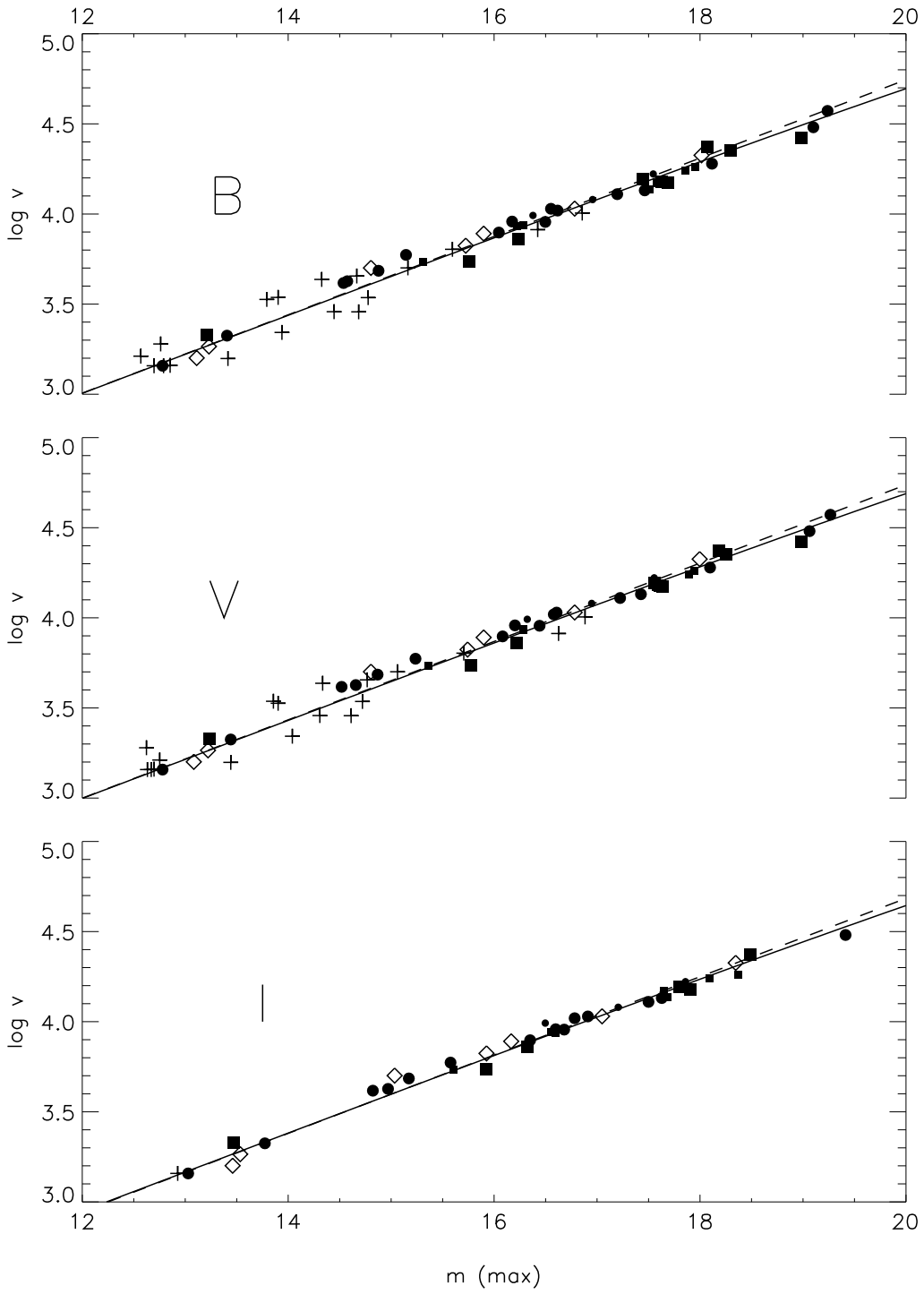

fig.3

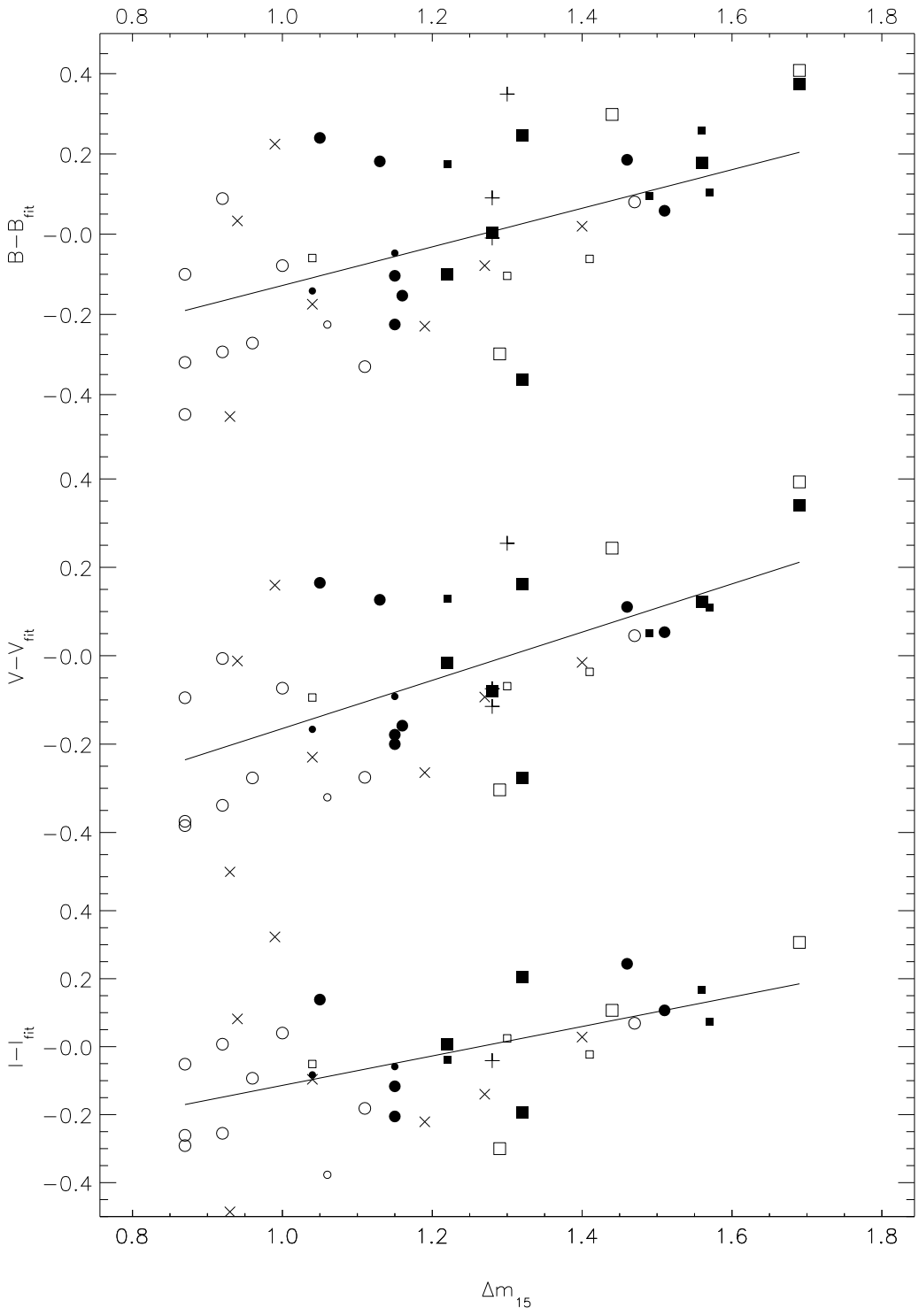

fig.4

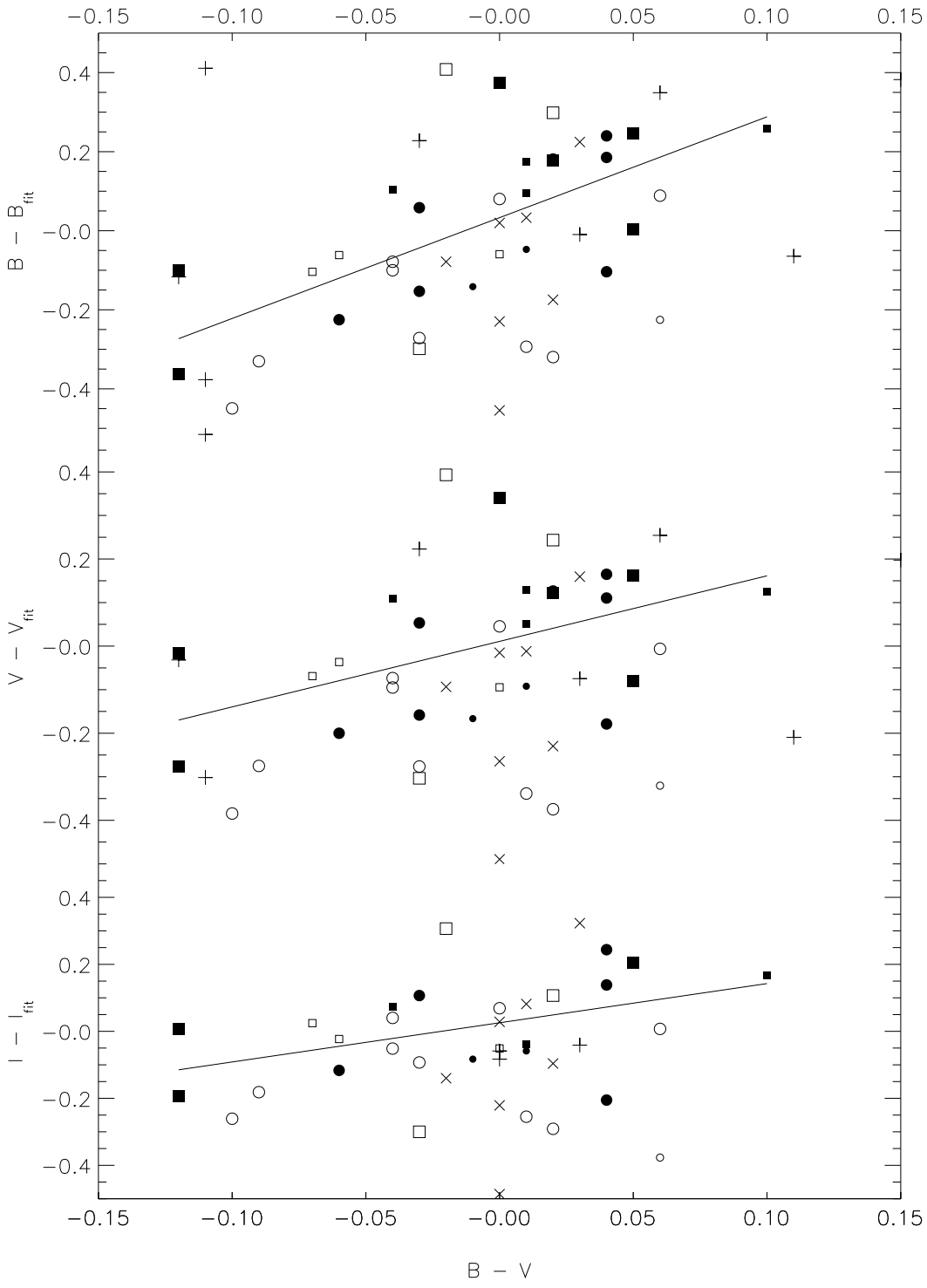

fig.5

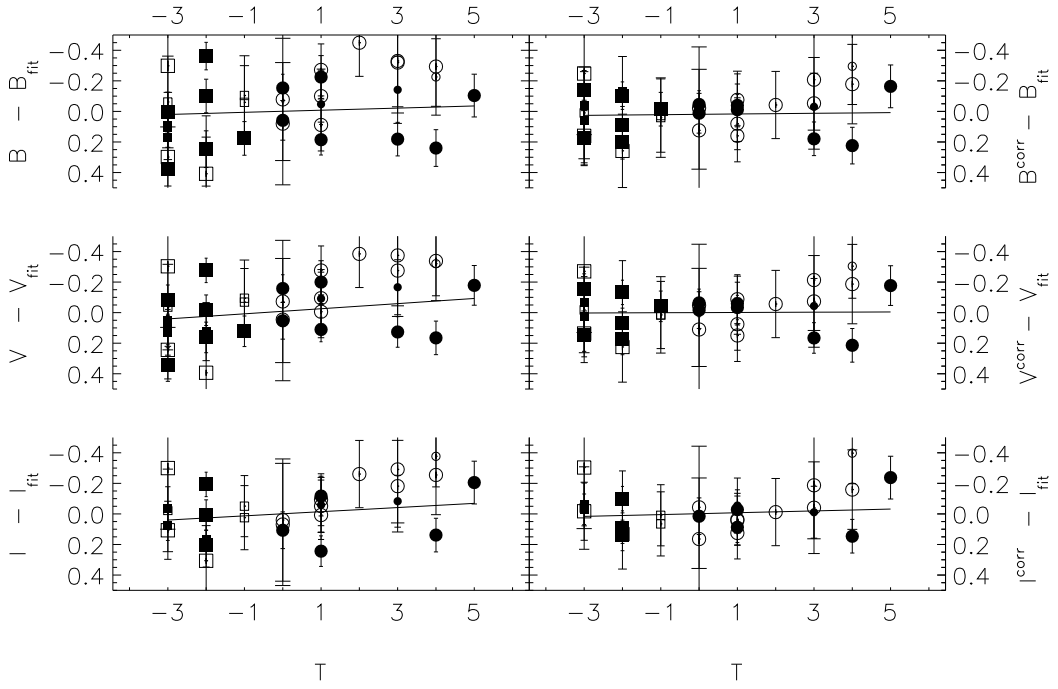
−3
−1
1
3
5
−0.4
−0.2
0.0
0.2
0.4
B − B_fit
V − V_fit
I − I_fit
B^corr − B_fit
V^corr − V_fit
I^corr − I_fit
T

fig.6

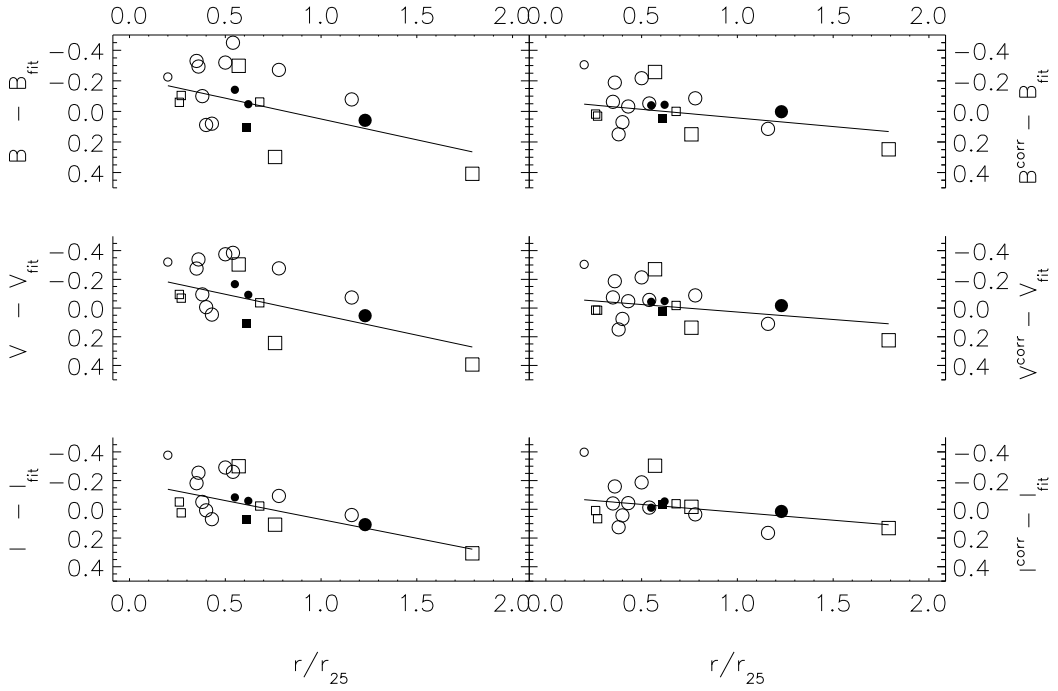
B − B_fit
V − V_fit
I − I_fit
B^corr − B_fit
V^corr − V_fit
I^corr − I_fit
r/r_25
r/r_25

fig.7

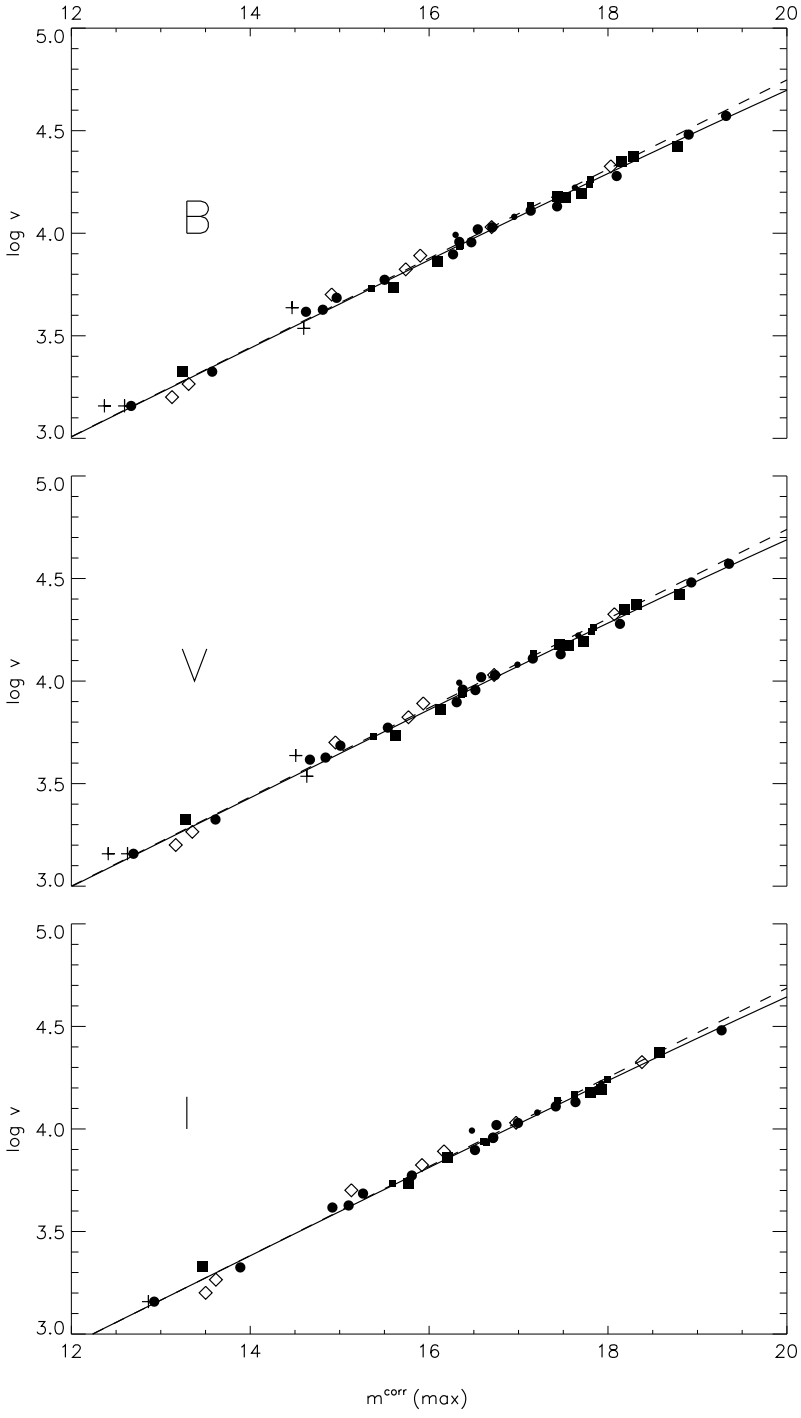

fig.8

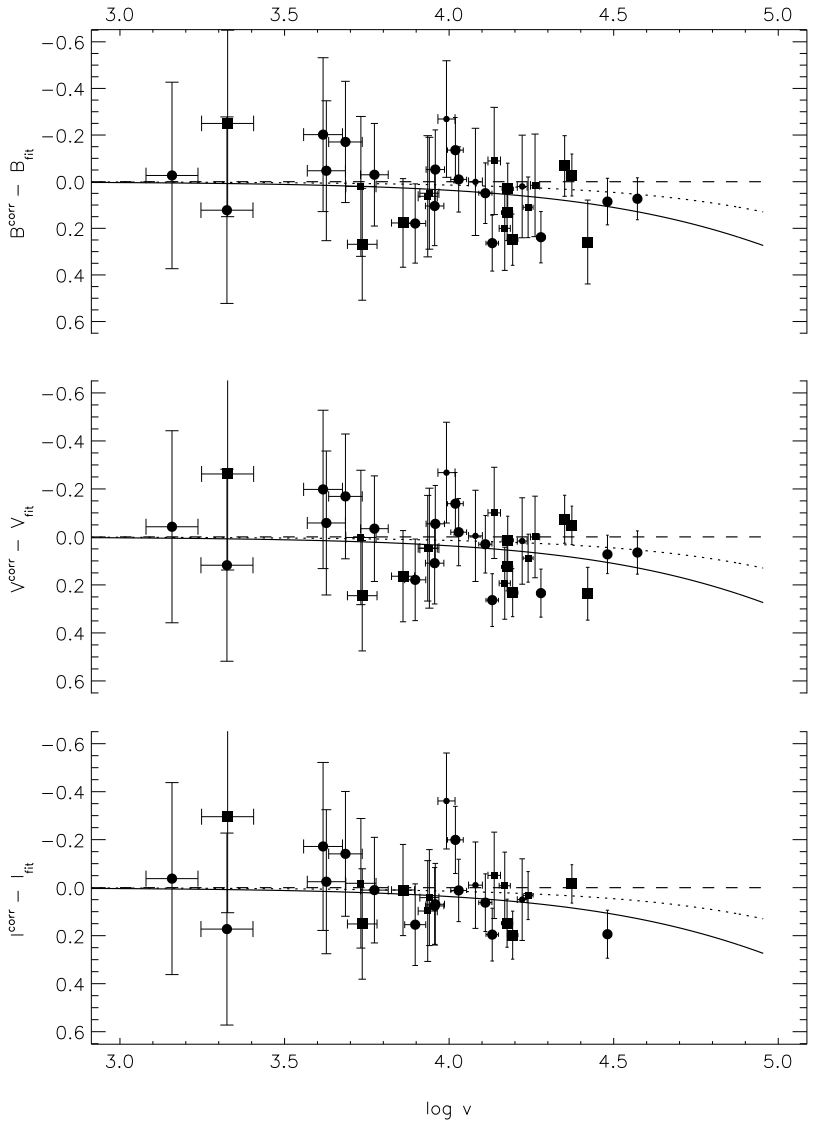
3.0
3.5
4.0
4.5
5.0
−0.6
−0.4
−0.2
0.0
0.2
0.4
0.6
$B^{corr} - B_{fit}$
$V^{corr} - V_{fit}$
$I^{corr} - I_{fit}$
log v

fig.9

Table 1. PHOTOMETRIC PARAMETERS OF BLUE SNE IA ((B-V) $\leq$ 0.20)

SN (1)	T (2)	log v (3)	B (4)	V (5)	I (6)	A_V (7)	Δm_{15} (8)	1st obs (9)	Ref. (10)	M_B^{60} (11)	M_V^{60} (12)	M_I^{60} (13)
1937 C	5	2.464(79)	8.74(09)	8.77(11)	...	0.05	0.87(10)	...	4a	—*	—*	...
1956 A	3	3.160(79)	12.58(30)	12.41(30)	...	0.10	...	+8:	2	-19.33(50)	-19.50(50)	...
1959 C	5	3.526(71)	13.60(20)	13.72(20)	...	0.09	...	+2:	2	-20.15(41)	-20.03(50)	...
1960 F	5	3.072(41)	11.49(10)	11.43(15)	...	0.08	1.06(12)	...	1	—*	—*	...
1962 A	-2	3.804(39)	15.56(40)	15.68(40)	...	0.04	...	-15:	2	-19.58(45)	-19.46(45)	...
1965 I	-1	3.211(79)	12.27(30)	12.47(30)	...	0.11	...	-10:	3	-19.90(50)	-19.70(50)	...
1966 K	-1	4.005(25)	16.93(40)	16.96(40)	...	0.06	...	-11:	2	-19.22(42)	-19.19(42)	...
1967 C	5	3.198(79)	13.19(30)	13.22(30)	...	0.09	...	0:	2	-18.91(50)	-18.88(50)	...
1969 C	5	3.537(70)	13.72(30)	13.67(30)	...	0.06	...	+5:	3	-20.08(46)	-20.13(46)	...
1970 J	-3	3.536(70)	14.67(30)	14.61(30)	...	0.26	1.30(..)	-12:	3	-19.13(46)	-19.19(46)	...
1971 G	1	3.343(79)	13.76(25)	13.87(25)	...	0.12	...	-17:	3	-19.07(47)	-18.96(47)	...
1971 L	3	3.279(79)	12.48(25)	12.33(25)	...	0.41	...	-5:	3	-20.03(47)	-20.18(47)	...
1972 E	5:	2.464(79)	8.25(14)	8.30(15)	8.68(00)	0.19	0.87(10)	...	4a	—*	—*	—*
1972 H	3	3.458(79)	14.31(40)	14.16(40)	...	0.08	...	+8:	3	-19.09(56)	-19.24(56)	...
1972 J	-1	3.457(79)	14.57(30)	14.49(30)	...	0.15	...	-9:	3	-18.83(50)	-18.91(50)	...
1973 N	5	3.656(54)	14.55(40)	14.66(40)	...	0.28	...	+5:	3	-19.85(48)	-19.74(48)	...
1975 O	3	3.701(49)	15.09(40)	14.98(40)	...	0.19	...	0:	3	-19.53(47)	-19.64(47)	...
1976 J	5	3.637(56)	14.18(30)	14.19(30)	...	0.09	0.90(..)	-2:	3	-20.12(41)	-20.11(41)	...
1980 N	1	3.158(79)	12.40(..)	12.37(..)	12.65(..)	0.07	1.28(04)	...	4	-19.49(50)	-19.52(50)	-19.24(50)
1981 D	1	3.158(79)	12.50(..)	12.33(..)	...	0.07	...	-15.5	5	-19.39(50)	-19.56(50)	...
1984 A	1	3.072(41)	12.36(25)	12.20(25)	...	0.11	1.20(..)	...	4	—	—	...
1990 N	3	3.072(41)	12.64(03)	12.62(02)	12.89(02)	0.09	1.05(05)	-14.0	6,8	—*	—*	—*
1990 O √	1	3.958(28)	16.19(10)	16.22(08)	16.65(09)	0.31	0.96(10)	0.0	4	-19.73(17)	-19.70(16)	-19.27(17)
1990 T √	1	4.080(21)	17.04(21)	17.03(16)	17.31(15)	0.18	1.15(10)	+16.0	4	-19.49(23)	-19.50(19)	-19.22(18)
1990 af √	-1	4.178(17)	17.77(07)	17.75(06)	...	0.12	1.56(05)	-3.0	4	-19.26(11)	-19.28(10)	...
1991 S √	3	4.222(15)	17.68(21)	17.69(16)	18.02(15)	0.09	1.04(10)	+13.0	4	-19.57(22)	-19.56(18)	-19.23(17)
1991 T	3	3.072(41)	11.70(06)	11.51(05)	11.67(05)	0.07	0.95(05)	-12.0	8	—	—	—
1991 U √	4	3.992(26)	16.41(21)	16.35(16)	16.54(15)	0.21	1.06(10)	+11.0	4	-19.68(25)	-19.74(21)	-19.55(20)
1991 ag √	3	3.617(59)	14.41(14)	14.39(15)	14.72(19)	0.21	0.87(10)	+7.0	4	-19.79(33)	-19.81(33)	-19.48(35)
1992 A √	0	3.158(79)	12.50(07)	12.50(06)	12.77(06)	0.06	1.47(05)	-8.0	4a	-19.40(40)	-19.40(40)	-19.13(40)
1992 J √	-2	4.137(19)	17.64(21)	17.54(16)	17.83(15)	0.19	1.56(10)	+14.0	4	-19.18(23)	-19.28(19)	-18.99(18)
1992 P √	1	3.897(32)	16.05(07)	16.09(06)	16.38(06)	0.08	0.87(10)	-1.0	4	-19.56(17)	-19.52(17)	-19.23(17)
1992 ae √	-3	4.351(11)	18.50(12)	18.45(08)	...	0.12	1.28(10)	+1.0	4	-19.40(13)	-19.45(10)	...
1992 ag	5	3.891(32)	16.23(08)	16.15(07)	16.34(06)	0.32	1.19(10)	-1.0	4	-19.35(18)	-19.43(17)	-19.24(17)
1992 al √	3	3.627(58)	14.45(07)	14.54(06)	14.88(06)	0.11	1.11(05)	-5.0	4	-19.80(30)	-19.71(30)	-19.37(30)
1992 aq √	1	4.481(08)	19.37(09)	19.33(07)	19.71(09)	0.04	1.46(10)	0.0	4	-19.20(10)	-19.24(08)	-18.86(10)
1992 au √	-3	4.261(14)	18.12(21)	18.11(16)	18.58(15):	0.06	1.49(10)	+12.0	4	-19.33(22)	-19.34(17)	-18.87(17):
1992 bc √	2	3.773(42)	15.07(07)	15.17(06)	15.54(05)	0.07	0.87(05)	-11.0	4	-19.91(22)	-19.81(22)	-19.44(22)
1992 bg √	1	4.029(24)	16.60(08)	16.66(07)	16.99(06)	0.61	1.15(10)	+5.0	4	-19.67(14)	-19.61(14)	-19.28(13)
1992 bh √	4	4.131(19)	17.59(08)	17.55(06)	17.77(06)	0.07	1.05(10)	-1.0	4	-19.20(12)	-19.24(11)	-19.02(11)
1992 bk √	-3	4.240(15)	18.02(10)	18.06(07)	18.27(06)	0.05	1.57(10)	+8.0	4	-19.32(13)	-19.28(10)	-19.07(10)
1992 bl √	0	4.110(20)	17.30(08)	17.33(07)	17.63(06)	0.04	1.51(10)	+2.0	4	-19.38(13)	-19.35(12)	-19.05(12)
1992 bo √	-2	3.736(45)	15.74(07)	15.76(06)	15.92(05)	0.09	1.69(05)	-8.0	4	-19.06(24)	-19.04(23)	-18.88(23)
1992 bp √	-2	4.373(11)	18.25(07)	18.37(06)	18.70(06)	0.23	1.32(10)	-2.0	4	-19.77(09)	-19.65(08)	-19.32(08)
1992 br √	-3	4.421(10)	19.24(17)	19.24(10)	...	0.09	1.69(10)	+5.0	4	-19.02(18)	-19.02(11)	...
1992 bs √	3	4.279(13)	18.30(09)	18.28(07)	...	0.04	1.13(10)	+2.0	4	-19.24(11)	-19.26(10)	...
1993 B	3	4.326(12)	18.48(11)	18.39(09)	18.68(10)	0.26	1.04(10)	+3.0	4	-19.30(13)	-19.39(11)	-19.10(12)
1993 O √	-2	4.193(16)	17.57(07)	17.69(06)	17.96(06)	0.18	1.22(05)	-6.0	4	-19.53(11)	-19.41(10)	-19.14(10)
1993 ac √	-3	4.169(17)	17.72(16)	17.71(12)	17.79(11)	0.54	1.22(10)	+8.1	7	-19.26(18)	-19.27(15)	-19.19(14)
1993 ae √	-3	3.732(46)	15.25(20)	15.31(16)	15.57(14)	0.13	1.41(10)	+12.8	7	-19.53(30)	-19.47(28)	-19.21(27)
1993 ag √	-2	4.176(17)	17.83(08)	17.78(06)	18.07(06)	0.37	1.32(10)	-2.0	4	-19.19(12)	-19.24(10)	-18.95(10)
1993 ah √	-1	3.935(29)	16.24(21)	16.31(16)	16.65(15)	0.07	1.30(10)	+11.0	4	-19.56(26)	-19.49(22)	-19.15(21)
1994 D	-1	3.072(41)	11.77(07)	11.80(06)	12.03(05)	0.07	1.27(10)	-8.0	4a,9	—	—	—
1994 M √	-3	3.860(35)	16.26(08)	16.24(07)	16.35(06)	0.08	1.44(10)	+0.5	7	-19.16(19)	-19.18(19)	-19.07(19)
1994 Q √	-1	3.940(29)	16.31(19)	16.31(20)	16.60(14)	0.06	1.04(10)	+12.2	7	-19.51(24)	-19.51(25)	-19.22(20)
1994 S √	4	3.685(51)	14.78(07)	14.77(06)	15.10(06)	0.07	0.92(10)	-3.6	7	-19.76(26)	-19.77(26)	-19.44(26)
1994 T	1	4.030(24)	17.24(09)	17.15(08)	17.32(07)	0.10	1.40(10)	+2.2	7	-19.04(15)	-19.13(14)	-18.96(14)
1994 ae	5	3.201(79)	13.07(07)	12.99(06)	13.34(05)	0.10	0.99(05)	-12.1	7	-19.05(40)	-19.13(40)	-18.78(40)
1995 D √	0	3.325(79)	13.18(07)	13.22(06)	13.58(06)	0.19	1.00(05)	-2.6	7,10	-19.56(40)	-19.52(40)	-19.16(40)
1995 ac	1:	4.166(17)	17.08(07)	17.10(06)	17.28(06)	0.14	1.01(05)	-4.4	7	-19.89(11)	-19.87(10)	-19.69(10)
1995 ak	1:	3.824(37)	16.15(10)	16.07(09)	16.13(08)	0.13	1.27(10)	+3.7	7	-19.09(21)	-19.17(21)	-19.11(20)
1995 al	1:	3.265(79)	13.31(07)	13.22(06)	13.47(06)	0.05	0.94(05)	-3.9	7	-19.13(40)	-19.22(40)	-18.97(40)
1996 C √	1	3.956(28)	16.54(10)	16.48(10)	16.74(08)	0.05	0.92(10)	+4.0	7	-19.37(17)	-19.43(17)	-19.17(16)
1996 X √	-3	3.327(79)	12.97(07)	13.00(07)	13.25(07)	0.23	1.29(05)	-1.7	7	-19.78(40)	-19.75(40)	-19.50(40)
1996 ab √	1:	4.572(07)	19.52(08)	19.55(08)	...	0.11	1.16(10)	+3.3	7	-19.51(09)	-19.48(09)	...
1996 bl √	5	4.019(24)	16.67(07)	16.63(06)	16.85(07)	0.31	1.15(10)	-2.2	7	-19.55(14)	-19.59(13)	-19.37(14)

Table 1—Continued

SN (1)	T (2)	$\log v$ (3)	B (4)	V (5)	I (6)	A_V (7)	Δm_{15} (8)	1^{st} obs (9)	Ref. (10)	M_B^{60} (11)	M_V^{60} (12)	M_I^{60} (13)
1996 bv	1:	3.701(49)	15.33(13)	15.19(10)	15.24(09)	0.35	0.93(10)	+5.2	7	-19.29(28)	-19.43(26)	-19.38(26)

References. — (1) Saha et al. 1996b; (2) Leibundgut et al. 1991b; (3) Patat et al. 1997; (4) Hamuy et al. 1996b; (4a) Hamuy et al. 1996a; (5) Hamuy et al. 1991; (6) Leibundgut et al. 1991a; (7) Riess et al. 1999, light-curve template-fitting by us (as prescribed in Hamuy et al. 1996b, 1996c); (8) Lira et al. 1998; (9) Wu et al. 1995; Richmond et al. 1995; Patat et al. 1996; (10) Sadakane et al. 1996.

Note. — An acceptance sign $\surd$ behind the SN name marks a SN that is belonging to the fiducial sample. An asterisk * indicates a calibrator whose Cepheid-based absolute magnitude is given in Table 3.

Table 2. Host Galaxy and Positional Parameters of Blue SNe Ia

SN (1)	Galaxy (2)	Type (3)	T (4)	α (5)	δ (6)	D_{25} (7)	E/W (8)	N/S (9)	r_{offset}/r_{25} (10)
1895B	NGC 5253	Am	5:	133956	-313841	301	+16	+23	0.19
1937 C	IC 4182	Im	5	130545	+373621	362	+30	+40	0.28
1956 A	NGC 3992	Sb	3	115736	+532231	455	+67	-9	0.30
1959 C	UGC 8263	Sc	5	131123	+032442	81	+7	-3	0.19
1960 F	NGC 4496A	Sc	5	123140	+035621	238	+38	+24	0.38
1962 A	MCG 5-31-132	E/S0	-2	130636	+275224	49	-11	+7	0.53
1965 I	NGC 4753	S0p	-1	125223	-011157	362	-98	+68	0.66
1966 K	UGC 6322	S0p:	-1	111812	+281600	83	-26	+15	0.72
1967 C	NGC 3389	Sc	5	104828	+123201	165	-43	+44	0.75
1969 C	NGC 3811	Sc	5	114116	+474135	131	+9	+6	0.17
1970 J	NGC 7619	E	-3	232015	+081223	151	-27	-30	0.53
1971 G	NGC 4165	Sa	1	121212	+131448	72	+3	-30	0.84
1971 L	NGC 6384	Sb	3	173225	+070337	370	+27	+20	0.18
1972 E	NGC 5253	Am	5:	133956	-313841	301	-38	-100	0.71
1972 H	NCG 3147	Sb	3	101653	+732404	256	+31	+37	0.38
1972 J	NGC 7634	S0	-1	232142	+085314	74	-5	-30	0.82
1973 N	NGC 7495	Sc	5	230854	+120200	109	-14	-7	0.29
1974 G	NGC 4414	Sc	5	122627	+311329	228	+27	-56	0.54
1975 O	NGC 2487	Sb	3	075820	+250859	154	+26	+15	0.39
1976 J	NGC 977	S:	5	023304	-104536	117	-10	-25	0.73
1980 N	NGC 1316	Sap	1	032242	-371227	721	+220	-20	0.61
1981 B	NGC 4536	Sbc	4	123427	+021119	455	+41	+41	0.25
1981 D	NGC 1316	Sap	1	032242	-371227	721	-20	-100	0.28
1984 A	NGC 4419	Sa	1	122657	+150252	199	-15	+30	0.34
1989 B	NGC 3627	Sb	3	112014	+125942	547	-15	+50	0.19
1990 N	NGC 4639	Sb	3	124253	+131531	165	+63	-2	0.76
1990 O	MCG 3-44-03	Sa	1	171533	+161842	52	+20	-3	0.78
1990 T	PGC 63925	Sa	1	195900	-561530	81	+25	-2	0.62
1990 af	Anon 2135-62	S0	-1	213500	-624400	...	-7	+7	...
1991 S	UGC 5691	Sb	3	102932	+215937	64	+4	+17	0.55
1991 T	NGC 4527	Sb	3	123409	+023913	370	+26	+45	0.28
1991 U	IC 4232	Sbc	4	132322	-260639	67	-3	+6	0.20
1991 ag	IC 4919	Sb	3	200009	-552228	89	-3	+22	0.50
1992 A	NGC 1380	S0/a	0	033627	-345833	287	-3	+62	0.43
1992 J	Anon 1009-26	E/S0	-2	100900	-263900	...	-11	+13	...
1992 P	IC 3690	Sa	1	124250	+102134	66	-6	+11	0.38
1992 ae	Anon 2128-61	E	-3	212818	-613300	...	+3	+5	...
1992 ag	ESO 508-G67	S:	5	132410	-235243	61	-4	0	0.13
1992 al	ESO 234-G69	Sb	3	204554	-512332	125	+18	-12	0.35
1992 aq	Anon 2304-37	Sa	1	230436	-372100	...	+2	-7	...
1992 au	Anon 0010-49	E	-3	001036	-49560	...	+21	+9	...
1992 bc	ESO 300-G9	Sab	2	030516	-393337	59	+15	+5	0.54
1992 bg	Anon 0741-62	Sa	1	074154	-623100	...	-3	+6	...
1992 bh	Anon 0459-58	Sbc	4	045930	-585000	...	+1	-2.5	...
1992 bk	ESO 156-G8	E	-3	034301	-533815	79	+12	+21	0.61
1992 bl	ESO 291-G11	S0/a	0	231512	-444414	43	+15	-22	1.23
1992 bo	ESO 352-G57	E/S0	-2	012202	-341150	81	-47	-55	1.79
1992 bp	Anon 0336-18	E/S0	-2	033636	-182100	...	-6	-1.5	...
1992 br	Anon 0145-56	E0	-3	014542	-560500	...	+3	-7	...
1992 bs	Anon 0329-37	Sb	3	032930	-371600	...	-9	+4	...
1993 B	Anon 1034-34	Sb	3	103454	-342700	...	+1	+5	...
1993 O	Anon 1331-33	E/S0	-2	133106	-331200	...	-14	+8	...
1993 ac	PGC 17787	E	-3	054616	+632110	...	-5	+31	...
1993 ae	UGC 1071	E	-3	012945	-015831	83	+16	+23	0.68
1993 ag	Anon 1003-35	E/S0	-2	100336	-352800	...	-5	-6	...
1993 ah	ESO 471-G27	S0	-1	235151	-275748	60	-1	+8	0.27
1994 D	NGC 4526	S0	-1	123403	+074201	435	-9	+7	0.05
1994 M	NGC 4493	E	-3	123108	+003648	74	+3	-28	0.76
1994 Q	PGC 59076	S0	-1	164951	+402559	32	-1	-4	0.26
1994 S	NGC 4495	Sbc	4	123123	+290813	83	-13	-7	0.36
1994 T	PGC 46640	Sa	1	132129	-020941	...	+4	-12	...
1994 ae	NGC 3370	Sc	5	104704	+171626	190	-30	+6	0.32
1995 D	NGC 2962	S0/a	0	094054	+051000	158	+11	-91	1.16
1995 ac	Anon 2245-08	S:	1	224542	-084500	...	-1	-1	...
1995 ak	IC 1844	S:	1	024549	+031348	47	-7	+1	0.30

Table 2—Continued

SN (1)	Galaxy (2)	Type (3)	T (4)	α (5)	δ (6)	D_{25} (7)	E/W (8)	N/S (9)	r_{offset}/r_{25} (10)
1995 al	NGC 3021	Sbc	4	095057	+333316	87	-15	-3	0.35
1996 C	MCG +08-25-47	Sa	1	135048	+492000	66	-2	+13	0.40
1996 X	NGC 5061	E0	-3	131805	-265010	213	-51	-32	0.57
1996 ab	Anon 1521+27	S:	1	152106	+275500	...	+2:	+1:	...
1996 bl	Anon 0036+11	Sc	5	003617	+112340	...	-3	+6	...
1996 bv	UGC 3432	Scd:	5	061612	+570200	100	-2	+2	0.06
1998 bu	NGC 3368	Sab	2	104645	+114917	456	+4	+55	0.24

Table 3: Absolute B, V, and I magnitudes of blue SNe Ia calibrated through Cepheid distances of their parent galaxies

SN	Galaxy	$\log v^{a}$	$(m\text{-}M)_{AB}$	$(m\text{-}M)_{AV}$	$(m\text{-}M)^{0}$	ref.	B_{AB}	V_{AV}	I_{AV}	ref.
(1)	(2)	(3)	(4)	(5)	(6)	(7)	(8)	(9)	(10)	(11)
1895 B	NGC 5253	2.464[b]	28.13(08)	28.10(07)	···	2	8.26(20)	···	···	9
1937 C	IC 4182	2.519	28.36(09)	28.36(12)	···	1	8.80(09)	8.82(11)	···	10
1960 F	NGC 4496A	3.072[c]	31.16(10)	31.13(10)	···	3	11.60(15)	11.51(20)	···	3
1972 E	NGC 5253	2.464[b]	28.13(08)	28.10(07)	···	2	8.49(14)	8.49(15)	8.80(19)	10
1974 G	NGC 4414	2.820	···	···	31.46(17)	4	12.48(05)	12.30(05)	···	11
1981 B	NGC 4536	3.072[c]	···	···	31.10(12)	5	12.03(03)	11.93(03)	···	10
1989 B	NGC 3627	2.734	···	···	30.22(12)	6	12.34(05)	12.02(05)	11.75(05)	12
1990 N	NGC 4639	3.072[c]	···	···	32.03(22)	7	12.75(03)	12.71(02)	12.94(02)	10,13
1998 bu	NGC 3368	2.814[d]	···	···	30.37(16)	8	12.18(03)	11.88(03)	11.67(05)	14

SN	E_{B-V}	ref.	B^{0}	V^{0}	I^{0}	M_B^0	M_V^0	M_I^0	Δm_{15}
(1)	(12)	(13)	(14)	(15)	(16)	(17)	(18)	(19)	(20)
1895 B	···	···	···	···	···	-19.87(22)	···	···	···
1937 C	···	···	···	···	···	-19.56(15)	-19.54(17)	···	0.87(10)
1960 F	···	···	···	···	···	-19.56(18)	-19.62(22)	···	1.06(12)
1972 E	···	···	···	···	···	-19.64(16)	-19.61(17)	-19.27(20)	0.87(10)
1974 G	0.16(07)	11	11.79(31)	11.77(24)	···	-19.67(34)	-19.69(27)	···	1.11(06)
1981 B	0.10(03)	5	11.60(13)	11.60(10)	···	-19.50(18)	-19.50(16)	···	1.10(07)
1989 B	0.37(03)	12	10.75(14)	10.80(11)	11.01(08)	-19.47(18)	-19.42(16)	-19.21(14)	1.31(07)
1990 N	0.026(03)	15	12.64(13)	12.62(10)	12.89(09)	-19.39(26)	-19.41(24)	-19.14(23)	1.05(05)
1998 bu	0.365(06)	14	10.61(26)	10.68(20)	10.94(13)	-19.76(31)	-19.69(26)	-19.43(21)	1.08(05)
			mean (straight, excl. SN 1895 B)			-19.57(04)	-19.56(04)	-19.26(06)	1.06(05)
			mean (weighted, excl. SN 1895 B)			-19.55(07)	-19.53(06)	-19.25(09)	1.08(02)

[a] The velocities used are corrected for Virgocentric infall assuming a local infall velocity of 220 $\mathrm{km\,s^{-1}}$

[b] The mean velocity v=291 $\mathrm{km\,s^{-1}}$ of the Cen A group is used

[c] The mean velocity v=1179 $\mathrm{km\,s^{-1}}$ of the Virgo group is used

[d] The mean velocity v=652 $\mathrm{km\,s^{-1}}$ of the Leo group is used

References. — (1) Saha et al. 1994; (2) Saha et al. 1995; (3) Saha et al. 1996b; (4) Turner et al. 1998 ; (5) Saha et al. 1996a; (6) Saha et al. 1999; (7) Saha et al. 1997; (8) Tanvir et al. 1995; (9) Schaefer 1995; (10) Hamuy et al. 1996a; (11) Schaefer 1998; (12) Wells et al. 1994; (13) Lira et al. 1998; (14) Suntzeff et al. 1999; Jha et al. 1999; (15) Schlegel, Finkbeiner, & Davies 1998.

Table 4: Intrinsic colors of unreddened blue SNe Ia after 1985

	(B-V)	n	(V-I)	n
SNe Ia in E/S0s	-0.013(015)	16	-0.240(024)	12
SNe Ia in spirals with $r/r_{25} \geq 0.4$ and (B-V)$\leq$0.06	-0.013(015)	9	-0.326(018)	9
Calibrators	-0.009(015)	8	-0.270(027)	4
mean	-0.012(008)	33	-0.276(016)	25
other SNe Ia in spirals	-0.001(016)	10	-0.288(024)	8

Table 5: Reddened SNe Ia of the present sample

SN	r/r_{25}	(B-V)	(V-I)	<E(B-V)>	B^0	V^0	I^0	M_B^{60}	M_V^{60}	M_I^{60}
(1)	(2)	(3)	(4)	(5)	(6)	(7)	(8)	(9)	(10)	(11)
1992 ag	0.13	0.08	-0.19	0.079	15.89	15.89	16.18	-19.67	-19.67	-19.38
1993 B	···	0.09	-0.29	0.067	18.19	18.17	18.55	-19.55	-19.57	-19.19
1994 T	···	0.09	-0.17	0.090	16.85	16.85	17.14	-19.41	-19.41	-19.12
1994 ae	0.32	0.08	-0.35	0.049	12.86	12.83	13.24	-19.25	-19.28	-18.87
1995 ak	0.30	0.08	-0.06	0.105	15.70	15.72	15.92	-19.53	-19.51	-19.31
1995 al	0.35	0.09	-0.25	0.074	12.99	12.98	13.32	-19.44	-19.45	-19.11
1996 bv	0.06	0.14	-0.05	0.147	14.70	14.70	14.95	-19.91	-19.91	-19.66